CORRELATING THE SPATIAL DISTRIBUTION OF SNOW DEPTH TO FOREST CANOPY PARAMETERS DERIVED FROM TERRESTRIAL LASER SCANS

by

Zachary Uhlmann

A thesis

submitted in partial fulfillment

of the requirements for the degree of

Master of Science in Geoscience

Boise State University

December 2018

BOISE STATE UNIVERSITY GRADUATE COLLEGE

DEFENSE COMMITTEE AND FINAL READING APPROVALS

of the thesis submitted by

Zachary Uhlmann

Thesis Title: Correlating the Spatial Distribution of Snow Depth to Forest Canopy Parameters Derived from Terrestrial Laser Scans

Date of Final Oral Examination: 7 November 2018

The following individuals read and discussed the thesis submitted by student Zachary Uhlmann, and they evaluated his presentation and response to questions during the final oral examination. They found that the student passed the final oral examination.

Nancy F. Glenn, Ph.D.	Chair, Supervisory Committee
James P. McNamara, Ph.D.	Member, Supervisory Committee
Hans-Peter Marshall, Ph.D.	Member, Supervisory Committee

The final reading approval of the thesis was granted by Nancy F. Glenn, Ph.D., Chair of the Supervisory Committee. The thesis was approved by the Graduate College.

DEDICATION

To my wife for encouraging and tolerating me during this busy time, my son for giving me the joy of toddlerhood to look forward to at the end of the day, and to my parents and mother-in-law for babysitting all the time (among other things…).

ACKNOWLEDGEMENTS

I would like to acknowledge everybody who helped me to pursue my education and research goals over the past couple years. I was lucky to have a great committee, thanks to all of them. To Dr. Hans-Peter Marshall for multiple invaluable sessions explaining the nuts and bolts of geostatistics and snow, and much-needed reassurances that even simple results were important contributions to the field of snow hydrology. To Dr. James McNamara for excellent guidance on selecting knowledge gaps in hydrology to explore, and providing straightforward feedback as I progressed. To my advisor Dr. Nancy Glenn for her understanding and guidance, and for providing me with the opportunity to learn and grow amongst all the amazing students and colleagues in her seemingly limitless orbit. Thanks to all the students, and those in BCAL in particular, who helped me every day with my work. Big thanks to Lucas Spaete for collecting my data with a suboptimal intervertebral situation, processing data and helping immensely with analysis. Thanks to NASA EPSCoR for the funding (Award #NNX14AN39A), and to Dr. Alejandro Flores, the principal investigator, for providing my funding.

ABSTRACT

In nonpolar, cold climate zones, snow accounts for 17% of the total terrestrial water storage. Estimating the amount of water stored in a snowpack, the snow water equivalent (SWE), and its spatial distribution is crucial to providing water managers with parameters to predict runoff timing, duration and amount. Reservoir management, hydropower and flood forecasting depend on SWE estimates. While landscape features such as aspect and slope are dominant controls on radiative energy in non-forested areas, forest cover can shift the energy balance composition from turbulent exchange in exposed, windy sites to primarily radiative inputs in the subcanopy. Additionally, forest cover moderates wind speed, and hence snow redistribution, and intercepts snow during storm events. Shading from forest cover reduces the effect of solar radiation. Forests cover approximately half of the snow-covered landmasses on Earth during peak snow extent, therefore accounting for them in snow mass and energy balance models is critical. Classifying forest cover into structural characteristics that correlate to snow accumulation and melt processes can inform snow interception and melt models, and thus estimates of SWE. In this study, we use terrestrial laser scanning (TLS) data from the 2016/2017 NASA SnowEx field campaign in Grand Mesa, CO, to assess the effect of forest canopy on the spatial distribution of snow depth during the accumulation period, prior to significant melt.

TABLE OF CONTENTS

LIST OF TABLES

LIST OF FIGURES

LIST OF ABBREVIATIONS

SWE	Snow Water Equivalent
CIE	Canopy Interception Efficiency
SVF	Sky View Fraction

INTRODUCTION

Forest Controls on Snow Processes

Forests cover approximately half of the snow-covered landmasses on Earth during peak snow extent (Kim et al., 2017), with snow in nonpolar, cold climate zones accounting for 17% of the total terrestrial water storage (Rutter et al., 2009; Guntner et al., 2007). Estimating the amount of water stored in a snowpack, the snow water equivalent (SWE), and its spatial distribution under various physiographic conditions, is crucial to providing water managers with parameters to predict runoff timing, duration and amount. However, climate change has redefined historical weather patterns, including the spatial and temporal distribution and intensity of precipitation, and changes in the rain-snow transition (Nolin and Daly, 2006). An indirect result of this has been large-scale stand replacing events due to wildfire and mountain bark beetle infestation which significantly alter the hydrologic response (Bewley et al., 2010). Forest composition and cover will continue to change as this trend is projected to be sustained for decades at mid-latitudes globally (Moritz et al., 2012). Therefore, understanding the effect of forest structure on radiation partitioning and understory snow accumulation across various regions, synoptic weather regimes and spatial scales will be critical in adapting snow models to altered forest stands and regular occurrences of anomalous weather patterns (Lundquist et al., 2013).

Snow depth, density and their spatial distribution vary significantly between the forested and open landscapes in mountainous terrain. Snow accumulation under the forest

is affected by forest type and distribution, canopy cover, topography and other meteorological inputs like wind (interception loss) and insolation (sublimation). The subcanopy radiative regime, when integrated across an entire melt season, is a function of the climate (temperature and atmospheric insolation) and the tree distribution (Currier and Lundquist, in press; Seyednasrollah et al., 2013). The concept of a "radiative paradox" holds that the reduction in solar radiation from forest shading is oftentimes offset and even surpassed by longwave radiative enhancement (Sicart et al., 2004). As such, radiation input in the subcanopy is non-linearly correlated to the forest density and the degree of canopy cover – i.e. sky view fraction (SVF). Adding complexity to these nonlinear subcanopy energy inputs, is that canopy interception efficiency (CIE) responds differently to the same tree and forest stand characteristics which control subcanopy radiative energy exchange. Tree distribution, wind speed, air temperature and relative humidity, snow stickiness and density as well as branch and leaf stiffness can all govern the fraction of snow either lost to sublimation or deposited to the subcanopy floor. Net change in energy input to subcanopy snowpack must be reconciled with interception losses (Troendle & King, 1985) to measure the cumulative effect of forest canopy on net SWE input to a particular basin, watershed or hydrological unit of interest. Investigations into forest snow interactions characterize the canopy with quantitative measurements of canopy cover and density, like canopy closure and leaf area index (LAI) from hemispherical photos or remotely-sensed optical imagery (Hedstrom and Pomeroy, 1998).

Snow distribution patterns are also a reflection of wind redistribution, with snow drifts in certain environments containing a disproportionally large amount of SWE

relative to their area (Tinkham et al., 2013). In the open, snow distribution patterns during the accumulation period (non-forested areas) are largely a reflection of wind redistribution due to topographical roughness and shrub cover (Shook & Gray 1997; Trujillo et al., 2007; Deems et al., 2006). While global topographical parameters, i.e. static properties, like slope, aspect and curvature are correlated to areas of snow redistribution, indices which simulate wind redistribution built from these DEM parameters explain much more of the variation in snow depth than slope, aspect or curvature independently for example. Wind redistribution modeling utilizes either direct wind field models (Liston and Sturm, 1998), or terrain parameterizations (Winstral et al., 2002) with measured wind direction during storms. Terrain parameterizations adjust precipitation assigned to cells using statistical models by optimizing drift and scour patterns based on the relative position and inclination of a target cell (potential drift or scour location) to an upwind location. In relation to forest ecotones, the edges of forests are host to consistent inter-annual patterns of snow drifts (Hiemstra et al., 2006). In this case, vegetation is treated as ground in a digital surface model – "vegetation topography" (Deems et al., 2006), and snow drifting along forest edges is simulated similar to the effect of topography (Hiemstra et al., 2002). An alternative method to incorporate spatial SWE distribution patterns into a hydrological modeling framework is via snow-depletion curves, which scale SWE based on statistical relationships between measured snow depth points to fractional covered area in a given basin or area (Luce.et al., 1999).

A crucial step in representing forest snow interactions in snow models is characterizing the forest structure itself. Data for this research was collected during the accumulation period in mid-winter, and as such, this research will focus on snow

accumulation and redistribution; particularly how forest affects snow distribution in two areas with distinct snow distribution patterns: the open (non-forested areas) and the subcanopy. In the forest, we will explore the relationship between vertical canopy metrics with snow depth, to better constrain interception processes across various forest types, densities and spatial scales during mid-winter. Additionally, we will explore how snow in open areas is affected by its proximity and location in relation to the surrounding forest structure.

Thesis Organization

This thesis consists of two main studies. The remainder of this introductory chapter will summarize information common to both studies, including site description and data processing methods. The next two chapters are the two separate studies, followed by an overall conclusion. Both studies use data from the same research campaign, but not all the same sites. While separate topics, they focus on the effect of forest canopy on snow distribution. The first study investigates effects of forest edge on wind distribution in large canopy openings. To this effect, common topographic metrics (aspect, slope and curvature), and those characterizing the geographic position of the response variable (snow depth) in relation to the forest edge are assessed for evidence of wind redistribution using multilinear models. The second study compares snow depth distribution in the subcanopy to overhead canopy properties derived from TLS point clouds. Analysis is performed at multiple pixel sizes and at a larger, plot scale to thoroughly mine for correlation across multiple process scales.

SnowEx Campaign and Grand Mesa

SnowEx is an ongoing, multi-year NASA-led research campaign aimed at evaluating systems for remotely sensing snow properties, to inform future satellite deployments, with a primary focus of monitoring SWE across all snow climates and throughout the accumulation and melt. This research uses data collected during SnowEx Year 1 (2016-2017). The science goals for Year 1 were to: 1) Characterize the effect of forest cover on remote sensing retrievals. 2) Determine the effect of forest cover on snow depth and SWE variation. In fall 2016 and spring 2017, in-situ and remotely sensed data were collected across two main study areas - Grand Mesa and Senator Beck. Grand Mesa was selected as the primary study area due to its large range of canopy density, range in SWE, along with minimal slope and aspect. I will use TLS datasets from five ~ 300m diameter sites collected at Grand Mesa. Sites were scanned once in the fall, and at least one time during the winter.

Grand Mesa is a plateau which rises up 1.7 km from the surrounding region, with an area of approximately 470 km^2 and elevation ranging from 2922 m to 3440 m, rising along a west to east gradient. Vegetation on Grand Mesa follows an east/west gradient. Vegetation in the west, where wind speeds are highest, is comprised mostly of shrubs with patches of spruce and fir, the center portion of the mesa is semi-continuous forest cover consisting of fir and spruce interspersed with meadows, and in the east, where wind speeds are lowest, there is dense forest consisting of fir and spruce with some aspen (*Populus tremuloides*) at the lowest elevations. The dominant spruce and fir species across the mesa are Engelmann Spruce (*Picea engelmannii*) and subalpine fir (*Abies lasiocarpa*).

Meteorological data available for this analysis originated from two weather stations: West Mesa and Mid Mesa. West Mesa is situated beside Site A, at the western extent of forest cover on the plateau. Mid Mesa is next to Site M, in the center of the mesa, situated amidst denser forest.

Data Processing and Products

TLS Specifications and Scanning Logistics

Data from two separate field teams and instruments were used: Riegl VZ-1000 and Leica ScanStation C10. The main difference between them is the laser wavelength for each scanner. The Riegl has a 1550 nm laser, whereas the Leica has a 532 nm laser. Multiple scans (5-15 in the fall, 4-18 in the winter) were taken at each site and coregistered to produce a single point cloud for each collection date at each site. In the winter, scanning one site effectively took all day. In the fall, longer daylight hours and snow-free (quicker) scanner and reflector setup allowed for scanning of up to two sites a day, depending on the amount of forest cover. Individual scans were taken from 50 degrees off-nadir, to 150 degrees above nadir, in a 360 degree rotation at a 0.03 degree increment (angular resolution of 0.03 degrees) in both rotation planes with the Riegl scanner. Coregistered scans were then georegistered using surveyed locations within the plots with the scanner's proprietary software, RiSCAN. At most sites, each scan shared at least two GPS-surveyed 'tie points'. If quality or line of sight issues resulted in an inadequate number of tie points, then fixed objects (trees or build structures) were used instead. Global position coordinates (GPS) were collected with a Topcon HiPer V Real Time Kinematic (RTK) GPS for each tie point and the base station, with an accuracy of <1 cm. The base station coordinates were corrected for drift using the National Oceanic

and Atmospheric Administration Online Positioning User Service and tie points were adjusted to the updated base station coordinates. Scanning workflows were not available at this level of detail for the Leica, however it is known that the point density was thinned to 1 point/10cm^2 and points greater than 100m from the scanner were discarded.

Point Clouds to Rasters

The point clouds were classified into 'ground' and 'canopy' using Terrasolid (Bently MicroStation V8i). The classification algorithm begins with an initial triangular irregular networks (TIN) surface model and iteratively classifies ground points based their distance to the TIN plane and angle off TIN vertices. The remaining points are either classified as canopy or discarded as outliers based on distance, position and clustering criteria. After this initial classification, the canopy points were further filtered using the Cloth Simulation Filter (CSV; Zhang et al., 2016) within a point cloud processing software, CloudCompare (CloudCompare 2.8.1, 2016). This filtering step removed grass and low-lying vegetation to reduce classification confusion between forest and other vegetation. The CSV filter is similar to the ground/canopy classification routine from Terrasolid, but it uses rasters instead of TINs to classify ground and canopy using a height threshold. For instance, at Site K, points lower than 80cm were removed from the canopy, i.e. the canopy contained only points 80cm or greater.

Point clouds were conservatively subset (i.e. extents clipped) to avoid erroneous or ambiguous laser returns from occlusion, weak return signal, or beam divergence uncertainty. Sites were at a minimum, limited to points no more than 50m from each scan location. The point cloud was further manually cleaned at each site for each scan date.

Sections with line of site and occlusion issues from vegetation or topography were manually removed.

Using the classified point cloud, rasterized canopy height models were made using BCAL Lidar Tools (Streuker and Glenn, 2006). The general workflow to go from point cloud to pixel, involves binning all points from the TLS point cloud into grid cells of a specified size. Using the geographic extent of a site, it is divided into grid cells, and all points are binned into the grid cell in which they reside. Within each cell, multiple statistical measures were calculated for the canopy points. Raster sizes were $1m^2$ for the first manuscript (non-forested areas) and ranged from $0.25m^2$ to $3m^2$ for the second manuscript (subcanopy).

To calculate snow depth, a simple method commonly used in geomorphology to measure surface change, called DEMs of Difference (Schaffrath et al., 2015) was used. Alternative methods like Iterative Closest Point (Nissen et al., 2012) and direct point cloud differencing were also considered. For simplicity and in accordance with previous lidar snow studies (Deems et al., 2006; Trujillo et al., 2007), we used the DEMs of difference. For this method, two DEMs from the same site, one from fall and one winter, are georegistered together and differenced. The bare ground (fall) mean elevation is subtracted from the snow surface (winter) mean elevation, resulting in spatially explicit snow depth (Deems et al., 2013).

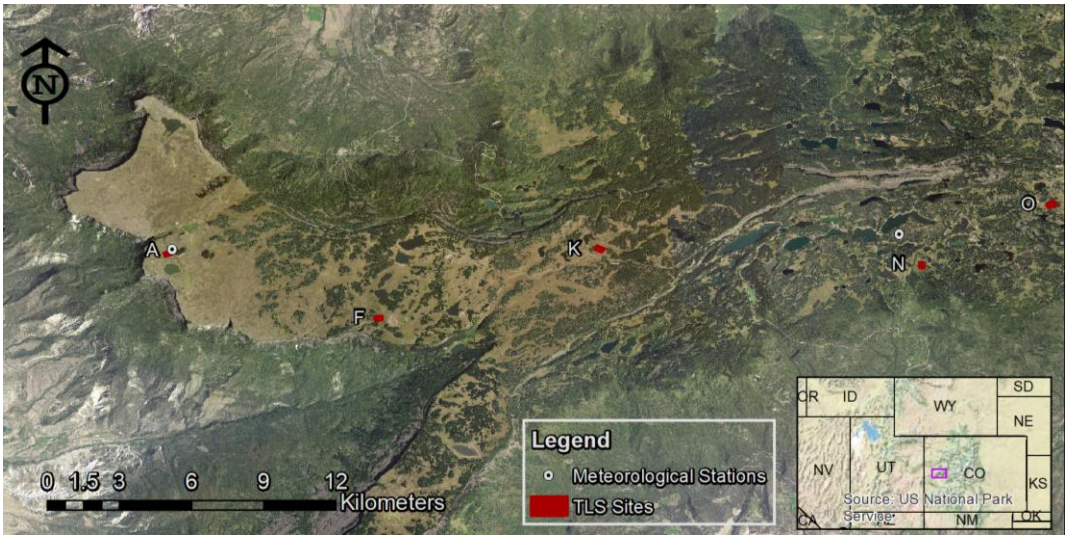

Figure 1.1: Study Area Map.

References

Bewley, D., Alila, Y., & Varhola, A. (2010). Variability of snow water equivalent and snow energetics across a large catchment subject to Mountain Pine Beetle infestation and rapid salvage logging, *Journal of Hydrology*, 388(3-4), 464-479.

Currier, W. R., & Lundquist, J. D. (in press). Snow depth variability at the forest edge in multiple climates in the western United States. *Water Resources Research.*

Deems, J. S., S. R. Fassnacht, & K. J. Elder (2006), Fractal distribution of snow depth from LIDAR data, J. *Hydrometeor*., 7(2), 285 - 297.

Deems, J. S., Painter, T. H., & Finnegan, D. C. (2013). Lidar measurement of snow depth: a review. *Journal of Glaciology*, *59*(215), 467-479.

Güntner, A., Stuck, J., Werth, S., Döll, P., Verzano, K., & Merz, B. (2007). A global analysis of temporal and spatial variations in continental water storage. *Water Resources Research*, *43*(5).

Hedstrom, N. R., & Pomeroy, J. W. (1998). Measurements and modelling of snow interception in the boreal forest. *Hydrological Processes*, *12*(10-11), 1611-1625.

Hiemstra, C.A., Liston, G.E., & Reiners, W.A. (2002). Snow redistribution by wind and interactions with vegetation at upper treeline in the Medicine Bow Mountains, Wyoming, U.S.A. Arctic. *Antarctic, and Alpine Research*, 34(3), 262-273.

Hiemstra, C. A., Liston, G. E., & Reiners, W. A. (2006). Observing, modelling, and validating snow redistribution by wind in a Wyoming upper treeline landscape. *Ecological Modelling*, 197(1-2), 35-51.

Kim, E., Gatabe, C., Hall, D., Newlin, J., Misakonis, A., Elder, K., & Entin, J. (2017, July). NASA's SnowEx campaign: Observing seasonal snow in a forested environment. Geoscience and Remote Sensing Symposium (IGARSS), 2017 IEEE International (pp.1388-1390). IEEE.

Liston, G.E., & Sturm, M. (1998). A snow-transport model for complex terrain. *Journal of Glaciology*, 44(148-516).

Luce, C. H., Tarboton, D. G., & Cooley, K. R. (1999). Sub-grid parameterization of snow distribution for an energy and mass balance snow cover model. *Hydrological Processes*, *13*(12-13), 1921-1933.

Lundquist, J. D., Dickerson-Lange, S. E., Lutz, J. A., & Cristea, N. C. (2013). Lower forest density enhances snow retention in regions with warmer winters: A global framework developed from plot-scale observations and modeling. *Water Resources Research*, 49(10), 6356-6370.

Moritz, M. A., Parisien, M. A., Batllori, E., Krawchuk, M. A., Van Dorn, J., Ganz, D. J., & Hayhoe, K. (2012). Climate change and disruptions to global fire activity. *Ecosphere*, 3(6), 1-22.

Nissen, E., Krishnan, A. K., Arrowsmith, J. R., & Saripalli, S. (2012). Three-dimensional surface displacements and rotations from differencing pre-and post-earthquake LiDAR point clouds. *Geophysical Research Letters*, *39*(16).

Nolin, A. W., & Daly, C. (2006). Mapping "at risk" snow in the Pacific Northwest. *Journal of Hydrometeorology*, 7(5), 1164-1171.

Rutter, N., Essery, R., Pomeroy, J., Altimir, N., Andreadis, K., Baker, B.,…Yamazaki, T. (2009). Evaluation of forest snow processes models (SnowMIP2). *Journal of Geophysical Research: Atmospheres*, 114(D6).

Schaffrath, K., Belmont, P., & J.M. Wheaton (2015), Landscape-scale geomorphic change detection; Quantifying spatially variable uncertainty and circumventing legacy data issues, *Geomorphology*, 250: 334-348.

Seyednasrollah, B., Kumar, M., & Link, T. E. (2013). On the role of vegetation density on net snow cover radiation at the forest floor. *Journal of Geophysical Research: Atmospheres*, *118*(15), 8359-8374.

Shook K & Gray D.M. (1997). Synthesizing shallow seasonal snow covers. *Water Resources Research*, 33(3), 419-426.

Sicart, J. E., Essery, R. L., Pomeroy, J. W., Hardy, J., Link, T., & Marks, D. (2004). A sensitivity study of daytime net radiation during snowmelt to forest canopy and atmospheric conditions. *Journal of Hydrometeorology*, 5(5), 774-784.

Streutker D., & N. Glenn. (2006). LiDAR measurement of sagebrush steppe vegetation heights. *Remote Sensing of Environment,* 102, 135-145.

Tinkham, W.T, Smith, A.M. S., Marshall, H.P., Link. T.E., Falkowski, M.J., & Winstral, A.H. (2013). Quantifying spatial distribution of snow depth errors from LiDAR using Random Forest. *Remote Sensing of Environment,* 141, 105-115.

Troendle, C. A., & King, R. M. (1985). The effect of timber harvest on the Fool Creek watershed, 30 years later. *Water Resources Research*, 21(12), 1915-1922.

Trujillo, E., Ramírez, J. A., & Elder, K. J. (2007). Topographic, meteorologic, and canopy controls on the scaling characteristics of the spatial distribution of snow depth fields. *Water Resources Research*, 43(7).

Winstral, A., Elder, K., & Davis, R.E. (2002). Spatial snow modelling of wind-redistributed snow using terrain-based parameters. *Journal of hydrometeorology*, 3(5), 524-538.

Zhang W, Qi J, Wan P, Wang H, Xie D, Wang X & G. Yan (2016), An Easy-to-Use Airborne LiDAR Data Filtering Method Based on Cloth Simulation, *Remote Sensing*, 8(6), 501.

EVALUATING WIND REDISTRIBUTION PROCESSES ALONG THE FOREST EDGE EXPLICTLY AND IMPLICITLY

Introduction

One of the most challenging components of modelling snow accumulation is accounting for wind redistribution of snow. While major components of snowmelt energy balance like solar irradiance and longwave radiation can be calculated using global parameters from DEMs (e.g. slope and aspect), along with measurements of temperature and estimates of cloud cover (Marks et al., 1998), wind redistribution requires much more a priori knowledge (training data) and optimization to be computationally-feasible and accurate. Early efforts to identify predictors of snow depth distribution in mountainous terrain which neglected wind redistribution of snow revealed that more than half of the variation in snow depth remained unexplained (Elder et al., 1991). The integration of snow redistribution into mass and energy balance snow models was a relatively late addition which greatly improved model skill. Winstral and Marks (2002) were able to explain 8-23% more of the variation in snow depth by incorporating a terrain parameter which integrates upwind conditions to estimate scour and deposition, using a "wind exposure index", to adjust the snow accumulation from each storm.

Terrain however is not the only physiographic cause of snow drifts. Snow redistribution along forest edges adheres to similar principles as those governing snow scour and deposition due to topography. As with concavities and leeward ridges, flow separation zones occur on the leeward edge of forests, making significant and persistent

snow drifts (Hiemstra et al., 2002). Snow distribution along forest edges is further affected by uneven radiative energy inputs due to solar shading from off-nadir solar declination angles during the ablation period. Webster et al. (2017) found significant differences in radiation loads and temperature ranges around canopy edges based on a forest edge's azimuth; wherein south-facing forest edges and those whose solar path is unimpeded by trees during the day receive more solar radiation than north-facing edges or those which are otherwise shaded. A recent study (Currier & Lundquist, in press) found that wind redistribution at the forest edge occurs at distances within three to ten times the average tree height of the surrounding forest, and the magnitude of snow drifting is a function of wind, climate and forest porosity.

Until the recent use of airborne lidar, large-scale remote sensing observations of snow distribution in mountainous terrain were limited to binary presence absence (Hall et al., 1995). Geostatistical analysis from lidar datasets both validated interpretations from transect and point based field data, and revealed large-scale trends linking depositional and melt processes to scales of the underlying physiography more comprehensively than was possible with point measurements. Trujillo et al. (2007) used lidar-derived snow and vegetation elevation data to correlate surface physiography like vegetation cover and topographical roughness to snow depth distributions using spectral analysis techniques over $1km^2$ "Intensive Study Areas" in the Colorado Rocky Mountains. In non-forested sites with moderate to heavy wind speeds, topographical roughness was the primary cause of snow depth variation. Using the same airborne lidar dataset as Trujillo, from NASA's Cold Land Processes Experiment in Colorado, Deems et al. (2006) were able to qualitatively link "vegetation topography" (topography + vegetation elevation)

distributions to snow depth distribution. They infer mechanisms which control snow distribution, including interception from vegetation canopy, wind redistribution due to vegetation topography and topography, and orographic effects (precipitation shadow).

This research will expand on this line of questioning by analyzing the snow distribution in open areas abutting forest edges, at high (meter) resolution over an approximately 300m extent, at multiple sites. Snow distributions from TLS sites across a gradient of wind and forest regimes will be explored to quantify relationships of snow patterns to forest edge metrics and commonly-used topographical predictors of snow distribution. Snow distribution adjacent to forest edges should reflect wind depositional processes and will be manifested in snow drifting and scour along forest edges concurrent with the prevailing winds.

Methods

Two Types of Metrics: Topographical and Edge

After the point clouds were processed and classified, rasters ($1m^2$) representing topography and forest canopy were created for use in analysis. Topographical rasters include elevation, slope, aspect and concavity and canopy metrics include distance from forest edge and edge direction (Table 2.1). Below are descriptions of each variable, followed by context for their inclusion in this analysis. Terrain parameterizations such as upwind slope and slope break (Winstral et al., 2002) were not used in this analysis as the site extents were too small to optimize these parameters to accurately represent the scale of wind depositional processes.

Topographical Metrics

Slope, aspect and concavity were calculated from the site DEMs. Concavity determines whether a location is relatively concave or convex (Shrivakshan and Chandrasekar, 2012), and is intended to be a general index of snow scour and deposition, independent of wind direction. All three of these topographic variables were derived from the fall scan, and therefore represent the bare ground topography, not the snow surface. Slope was calculated using a 3 X 3 Sobel 2D convolution kernel (Jähne, B. et al., 1999), to approximate the gradient magnitude. With gradient magnitudes from the above slope calculation, the aspect, or azimuth of the maximum slope was calculated, and ranged from 0° - 360°. The 3 X 3 Sobel is the same convolution kernel used with the ArcGIS Aspect and Slope Tools (ArcGIS 10.4.1 for Desktop). Topographical aspect was sinusoidal-transformed, specifically a cosine transformation. A north aspect of 0° would therefore be cos(0), or 1. This resulted in a range of values from -1 to 1 (Table 2.1).

Topographical concavity was calculated using a 2D convolution kernel, the Laplacian of the Gaussian (LoG), a filter commonly used in edge detection (Jähne et al., 1999). The LoG is the result of convolving a 3 X 3 Laplacian kernel with a Gaussian kernel parameterized by size and standard deviation (SD), which varied by site (values stated below). The Gaussian component smooths high frequencies that occur at smaller spatial scales than we would like concavity to be measured at, while the Laplacian approximates the second spatial derivative over the smoothed DEM. For this application, the LoG is used to classify the DEM pixels as either convex or concave, with an associated measure of magnitude. This is a continuous variable with fractional values both positive and negative prior to normalization.

Parameters for the LoG were chosen systematically by testing three combinations of filter parameters at each site to find the one with the greatest individual correlation to snow depth. Maximum size was constrained as to retain most grid cells along the edge of the forest. Increasing the size of the LoG filter shrunk the edges of the convolution product (concavity grid). This was because at each site there were places where the DEM barely extended past the forest edge, and grid cells convolved near the forest edge were assigned no value for concavity if there were not at least 50% DEM grid cells within the square LoG kernel window.

The LoG filter was optimized for each site to maximize variance of snow depth explained. Filter sizes tested included: 9x9m, 15x15m and 25x25m with SDs of 1, 2 and 3 respectively. Correlation to snow depth plateaued at 9x9m for Sites K and F. Site O showed better correlation up to 25x25m, however 15x15m was used as the larger kernels shrunk the site area to an unacceptable degree. Sites K and F used a LoG filter of size 9x9m with SD of 1. Site O was $15m^2$ with an SD of 2.

Topographical Spatial Scale

A limitation imposed by the use of topographic variables in this chapter was the requirement of continuous gridded data within the 3X3 moving window used to calculate slope and aspect; one grid cell with no data resulted in a nine-fold reduction in calculated slope and aspect grid cells. Therefore, the choice of grid size was bracketed by a desire for the finest resolution on one end, and an evenly-distributed rasterized dataset of variables on the conservative end. A visual examination of the slope and aspect maps created from the two DEMs showed an uneven spatial distribution for the smaller, $0.5m^2$

pixel size. Salvaging the $0.5m^2$ topographical data would require substantial interpolation or smoothing.

To ensure that the $1m^2$ pixels were not capturing noise from high frequency local slope patterns (rocks, holes, etc.), slope was calculated with coarser scale DEMs. At Site K, decreasing the spatial resolution of the DEM from $1m^2$ to $3m^2$ decreased the maximum slope value from 23º to 17º, and slightly improved the correlation to snow depth from 0.11 to 0.14 values of r^2. The $3m^2$ grid size was investigated at the remaining sites with similar results. Ultimately, the $1m^2$ resolution was chosen because it had a good spatial distribution and it was not noisy. Also, snow depth increased asymptotically moving away from the forest edge out to approximately 10 meters at Site K. We wanted to capture this variation with finer resolution distance increments.

Delineating Forest Edge

In order to create metrics defining spatial relationships of snow distribution to the forest edge, the forest was consolidated into larger polygon patches. Canopy rasters created in the BCAL Lidar Tools (Streuker and Glenn, 2006) were used to define areas of forest canopy. Pixels with a maximum height above 0.5m were defined as canopy, to avoid including misclassified forest canopy close to the ground. As seen from Figure 2.1, vegetation pixels are sometimes isolated or in small clusters. To avoid an unmanageable amount of tiny polygons, these outliers were aggregated into larger patches by reclassifying the canopy with an inverse distance squared moving window. This also helped to smooth discontinuous forest edges.

The workflow for aggregating forest patches is as follows:

1. A 2D moving window filter was passed over each pixel in the canopy raster, which is either classified as canopy or non-canopy (binary).
2. The weighted proportion of canopy classified grid cells within the moving window is calculated. Weights are assigned based on inverse distance squared weighting (Equation 1) from the target pixel.
3. If this weighted proportion is above a threshold (0.4), then the cell is reclassified as canopy.
4. Pixels classified as canopy cannot be reclassified as non-canopy.

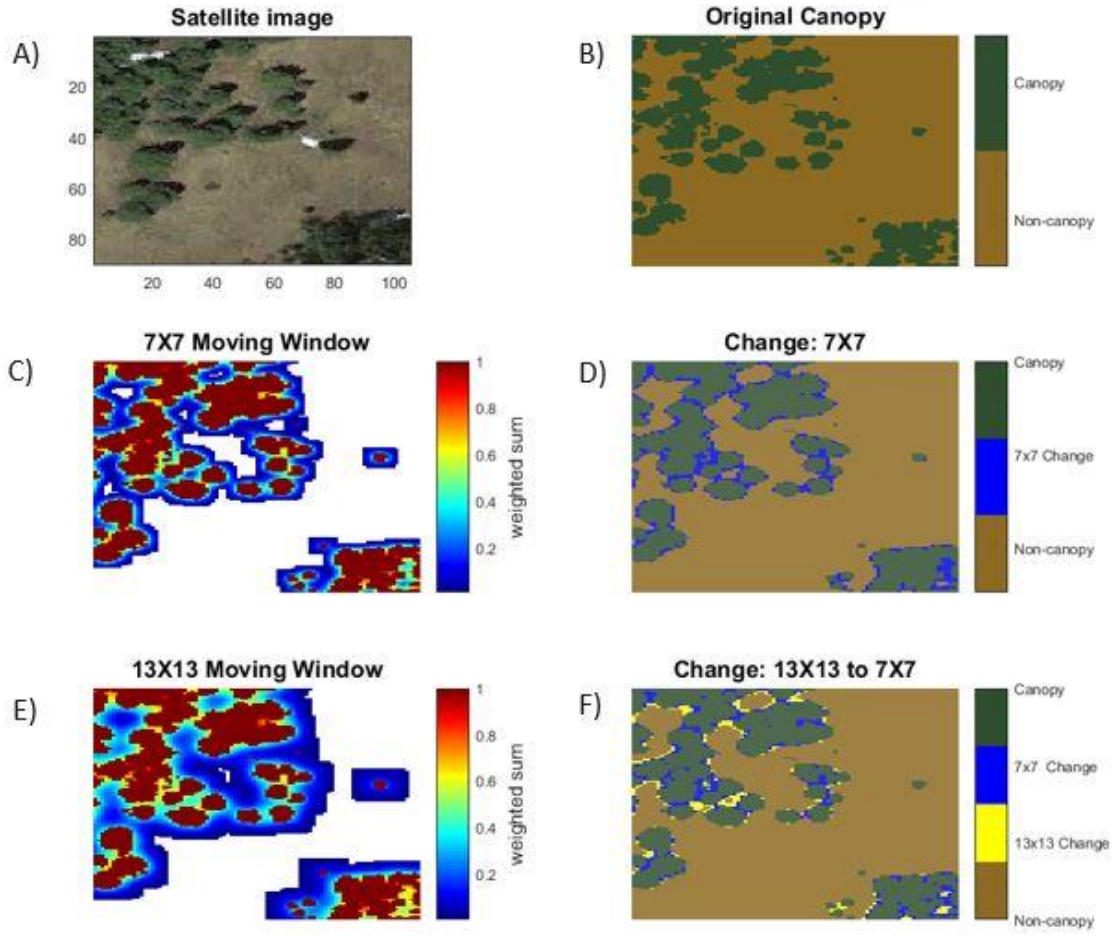

Figure 2.1: Effect of moving window parameters on a small sample (100 m x 100 m). Dimensions are in number of grid cells. Weighted sum refers to Zj from Equation 1 using inverse distance squared weighting. Threshold > 0.4 to classify as canopy. a) Site K, satellite image. b) Classification direct from point cloud. c) 7 X 7 moving window weighted sum. d) Classification of canopy including change with 7X7 moving window. d) 13X13 moving window weighted sum. f) Classification of canopy including change with 13X13 pixel window size.

Multiple combinations of window sizes and inverse distance weighting schemes (distance^2, distance$^{0.5}$, distance^3, etc.) were compared using Equation 1. The optimal window size and weighting scheme were ultimately chosen qualitatively, through trial and error. The goal was to ensure that forest edges were at most, minimally expanded. In the case of this dataset, a window-size of 7x7, with an inverse distance squared weighted scheme was found to preserve the original edge, and consolidate islands. A threshold of

0.4 was selected as it effectively aggregated small pixel clusters and smoothed the forest edge with minimal canopy reclassification. For instance, within the moving window centered on any pixel (position *j* from Equation 1), the weighted sum of pixels classified as canopy (Z_j) had to be 0.4 or greater to be reclassified from non-canopy to canopy.

$$Z_J = \frac{\sum_{i=1}^{N} W_{ij} * Z_i}{\sum_{i=1}^{N} W_{ij}}$$

Z_j is the weighted value at grid position *j*.
Z_i is the value at cell within window at position *i*. This is either 1 for canopy or 0 for non-canopy
W_i is the weight for cell within window at position *i*

Equation 1) Inverse distance weighting. If $Z_j > 0.4$, then cell is classified as canopy.

Once the pixels were reclassified, polygons were fit around canopy edges using ArcMAP (ArcGIS 10.4.1 for Desktop). This can be seen as the green outline in Figure 2.2 which will be discussed later.

Edge Metrics

Forest polygons were used to create two metrics relating the location of snow in the open to the closest forest edge: distance from edge and edge direction. Distance from edge is simply the distance of a grid cell in the open to the closest canopy edge, or the minimum distance away from a canopy edge. It will be referred to as "*distance"* throughout this manuscript. The second metric, edge direction, imputes the orientation of the closest edge to each grid cell in the domain. Orientation, or edge direction, refers to the normal direction of the line segment in the forest patch polygon, pointing away from the forest edge. Therefore, a forest edge on the west side of a patch, would have an edge direction of east. Directions were discretized into the eight sub-cardinal directions. They are intended as covariates of preferential wind deposition. Edge direction will be

shortened to "*edge"* throughout this thesis. Edge metrics, along with topographic metrics, were ultimately used as predictors for inferential snow depth models.

Snow Depth

Snow depth was calculated to match the spatial resolution of the topographic and edge metrics ($1m^2$) per the methods outlined in Chapter 1.

Statistical Analysis and Workflow

Analysis was performed on all pixels located outside of the canopy – i.e. in the "open" or non-forested areas within each site. Model selection utilized a cross-validation framework, using edge direction, distance to edge and topographic variables in linear and multilinear models. As a preliminary step to thin variables prior to model building, each metric was regressed against snow depth individually, and measures of model fit were evaluated. Variables with low individual correlation, coefficient of determinations (r^2) less than 0.01, and minimal improvement in correlation when interacted with other terms ($r^2<0.01$) were thinned prior to model selection. To test for non-linear interactions, the above step was repeated with transformed variables; distance was log-transformed and slope was both square-rooted and raised to the second and third power. At all sites, transformed slope had lower correlation to snow depth than the non-transformed slope and was not used in subsequent analysis. Grand Mesa was selected as a study area to control for slope, as such slope was minimal. Maximum slopes of 23º, 23º, and 31º were found at Sites K, F and O respectively. Slope is generally used in snow models as proxies for solar loading or as components of more complex snow drift and scour indices (Winstral et al., 2002).

After thinning variables with low correlation ($r^2<0.01$) and no interaction effect, each site had a different group of variables with which to build candidate models: Site O used all variables, Site K all but *slope*, and Site F used *distance, edge,* and *concavity*. At each site, every possible combination of remaining variables was combined into candidate models in the form of a multilinear regression against snow depth for each site (Tables 2.3, 2.4 and 2.5). Each variable was also individually regressed in a linear regression. 1,000 Monte Carlo simulations within a cross-validation framework were run for each model. For each Monte Carlo run the dataset was partitioned into 75% training and 25% testing data (75 to 25 partition). Each Monte Carlo simulation randomly sampled a subset from the entire dataset to train the model, with the remaining data used for testing. Data was replaced for each subsequent Monte Carlo run. For all models, the mean r^2 and root mean squared error (RMSE) of the 1,000 Monte Carlo simulations were used to measure model strength. Significance was assessed for each model, as well as all variables within each model using average p-values from the 1,000 simulations.

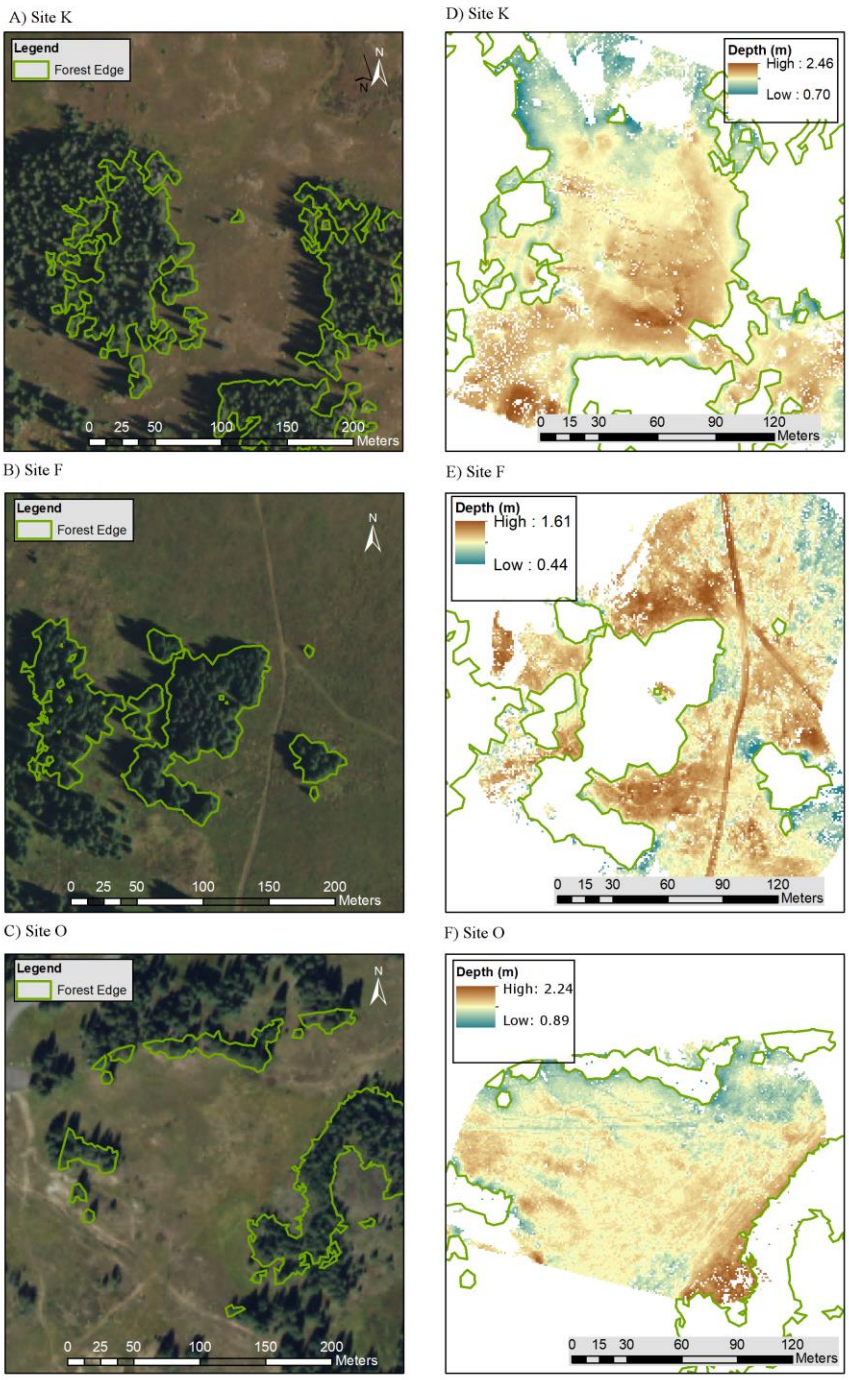

Figure 2.2: Aerial photos and snow depth maps for Sites K, F and O. Subplots a) – c) Aerial photos with delineated forest edges from point cloud extent. *Note: outer boundaries which delineate edge within forest are the furthest extent of point cloud perimeter. They have no snow depth on their border and are therefore not applicable to analysis. Subplots d) – f) Snow depth maps in the open.

Results

Correlation coefficients varied by site and model, and there was not a single variable that consistently showed relatively strong correlation to snow depth at all three. The best models were able to explain up to 40%, 39% and 64% of the variation in snow depth at Sites K, F and O, respectively. With most models, adding multiple variables together yielded an r^2 that was approximately the sum of the individual models – i.e. *distance* had an $r^2 = 0.01$ (p-value=0.01; Table 2.3), and *edge* had an $r^2 = 0.16$ (p-value = 0.00) for a sum of 0.17. Using these same variables as interaction coefficients with a *distance * edge* term yielded an r^2 of 0.28, or a 0.11 increase in r^2 from the additive model (Figure 2.3). In this case, each edge direction (N, NE, E, etc.) had its own associated intercept and slope, as opposed to *distance + edge* where each edge direction only varied by intercept with just one shared slope. At Site K for instance, snow depth from a southwestern facing edge (SW) would be modelled with: 151cm + 0.05 * *Dist* (p-value = 0.09 and 0.01 for intercept and slope respectively; Table A.1). A western facing edge (W) would be: 138cm + 0.10 * *Dist* (p-value = 0.01 and 0.15). The stated p-values are the result of Anova tests between the model for the specific direction in comparison to north facing (N) model for intercept and slope respectively.

This interaction effect between *distance* and *edge* was apparent at all sites to varying effect sizes (Tables 2.3, 2.4 and 2.5). Model performance also improved at Site O with the interaction of topographical metrics (Figure 2.3), particularly *slope * aspect*. The relative RMSE (RMSE normalized by the site mean) between modelled snow depth and measured snow depth ranged from 5 - 13.6% (Tables 2.3, 2.4 and 2.5) across all sites, and the increase in RMSE between the best and worst model at each site was 4 cm at most.

The RMSE of the constant model (i.e. mean snow depth) at each site was 17, 16 and 13cm for Sites K, F and O, respectively. These three values matched the RMSE of the worst performing models at each of the respective sites. Therefore, the models with the lowest RMSEs at each site showed no improvement over the constant model.

Model coefficients are listed in tables A.1, A.2 and A.3. Note that concavity is normalized to one standard deviation. For instance, in Table A.1, the coefficient for concavity is 6.9, which can be translated as: for every one SD of increased concavity, snow depth increased by 6.9cm. Distance is log-transformed (base e) for all sites except Site F where both distance and log distance had low correlation to snow depth ($r^2<0.02$), with slightly higher correlation using log-transformed distance, particularly when interacted with *edge* in *distance * edge*. *Edge* is a categorical variable, and therefore is not transformed.

Below are the results for each of the three sites used in this analysis.

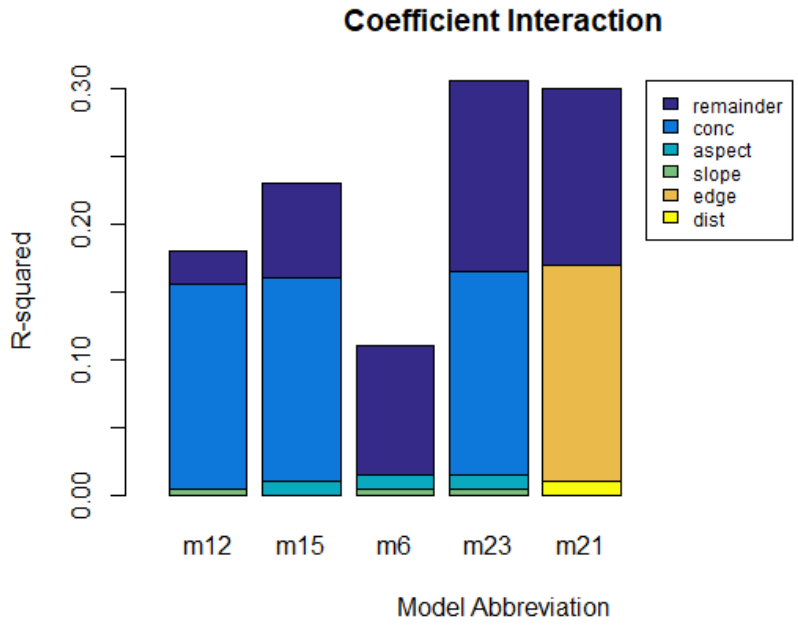

Figure 2.3: Site O Interaction. Total bar height is the r2 of the model with interaction. The different segments of the bar graph are the r2 value from one-to-one relationships. The remainder brings the r2 value to that of the model with each variable with interaction.

Table 2.1: Raster metrics derived from the point cloud.

Metric	Value Range (Site K)	Value Range (Site F)	Value Range (Site O)	Data Type
Cos (aspect)	-1 to 1	‘’	‘’	Continuous
Slope	0 – 22.4°	0.1 – 14.8 °	0.1 - 31.7 °	Continuous
Concavity	-0.038 – 0.025	-0.13 – 0.11	-1.58 – 4.83	Continuous
Distance from edge	0 - 46m	0 - 73m	0 - 66m	Continuous
Edge direction	N NE E SE S SW W NW	‘’	‘’	Discrete

Table 2.2: Snow depth statistics for each site.

Site	Mean (m)	Std (m)	Range (m)
K	1.70	0.13	0.70 – 2.46
F	1.18	0.14	0.44 – 1.61
O	1.59	0.09	0.89 – 2.24

Site K

Site K occurs in the forest at the edge of the ecotone from shrub-steppe to forest habitat. It has a nearly closed u-shaped open area surrounded by coniferous forest which opens facing north (Figures 2.2A and D). Snow scans of Site K were taken on February 22, 2017. It had the deepest snow depth of the three sites with a mean depth of 170cm (SD = 13cm; Table 2.2). *Distance* (log-transformed) from edge was the strongest predictor of snow depth (Table 2.3). Log transforming distance doubled the correlation from r^2 =0.11 to 0.22 compared with non-transformed distance, confirming the nonlinear relationship between snow depth and distance observed (Figures 2.5) The formula for the log distance model is: 1.43cm + 0.68 * *Log Distance* (log distance maximum is 3.82; distance maximum is 46m [Table 2.2]). Aside from distance, r^2 values for individual variables in predicting snow depth were low, 0.04 – 0.11 (Table 2.3). Intercepts were 8cm less on average for north-facing edges (N NE NW: p-values = 0.00, 0.00 and 0.29, respectively) than south-facing edges (S SE SW: p-values = 0.00, 0.01 and 0.00, respectively; Table A.1). Of all models tested, the most complex model which used every variable had the highest r-squared of 0.40. The range in RMSE for all models was 14-17cm (Relative RMSE = 8.9 - 10.8%). The constant model had an RMSE of 17cm.

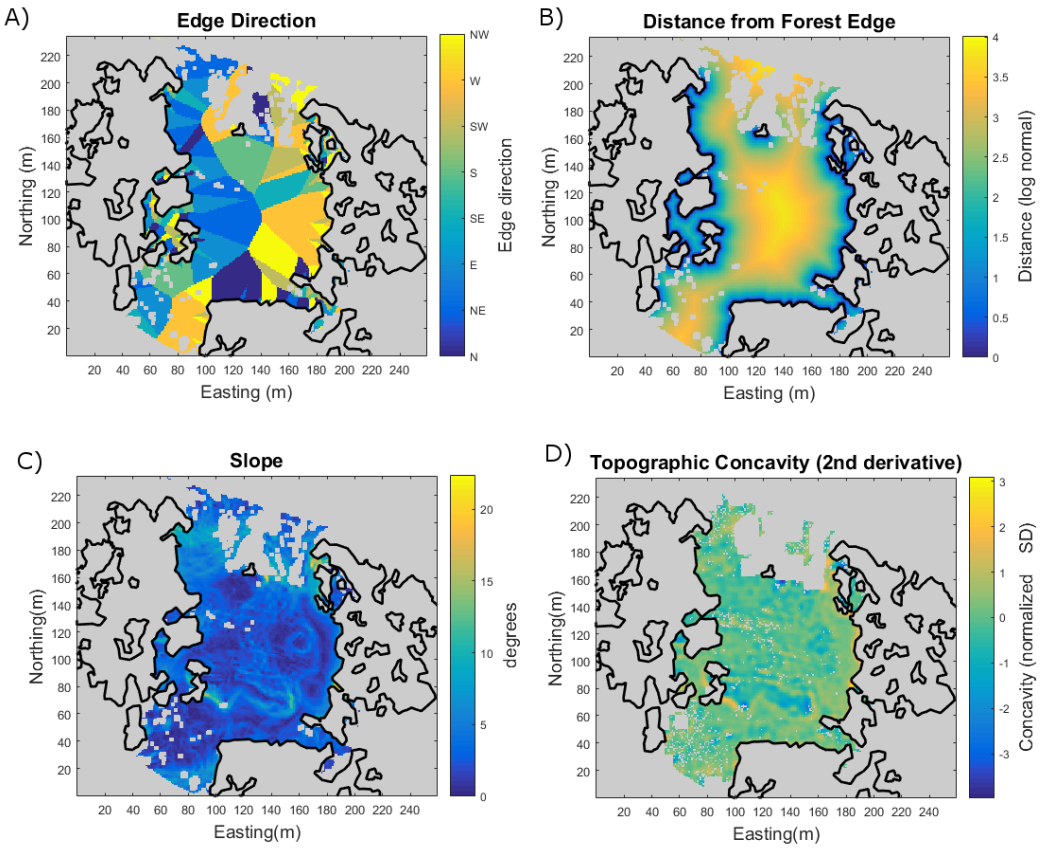

Figure 2.4: Site K selected metrics. a) Edge. b) Distance (log-transformed). c) Slope. d) Concavity.

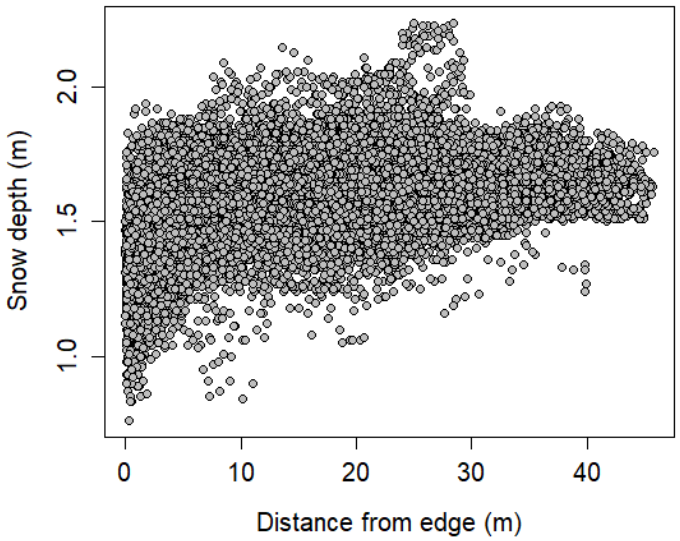

Figure 2.5. Non-transformed effect of distance from edge on snow depth at Site K (all pixels in the open; n=18,775 1m2 pixels).

Table 2.3: Results from model building process for Site K.

Model								R^2	RMSE	Relative RMSE (%)	P-value
15	Dist_log	*	Edge	+	Slope	+	Conc	0.40	0.14	8.9	0
14	Dist_log	*	Edge	+			Conc	0.35	0.14	8.9	0
13	Dist_log	*	Edge	+	Slope			0.34	0.14	8.9	0
12	Dist_log				Slope	+	Conc	0.31	0.14	8.9	0
11	Dist_log	*	Edge					0.30	0.15	9.5	0
10	Dist_log					+	Conc	0.26	0.15	9.5	0
9	Dist_log			+	Slope			0.25	0.15	9.5	0
8	Dist_log							0.22	0.15	9.5	0
7			Edge	+	Slope	+	Conc	0.18	0.16	10.1	0
6			Edge	+	Slope			0.16	0.16	10.1	0
5					Slope	+	Conc	0.14	0.16	10.1	0
4					Slope			0.11	0.16	10.1	0
3			Edge	+			Conc	0.05	0.17	10.8	0
2			Edge					0.04	0.17	10.8	0
1							Conc	0.02	0.17	10.8	0

Site F

Site F is located along the road, close to the southern edge of the plateau in the shrub-steppe to forest ecotone (Figures 2.2B, 2.2E and 1.1). The site has one large central forest patch with smaller patches along the periphery. TLS measurements were made on February 21, 2017. Mean snow depth was 118cm (SD = 14cm). *Concavity* had the strongest correlation of the three individual predictors (r^2 = 0.18, RMSE = 13cm; Table 2.4) at Site F. The constant model had a 16cm RMSE. Edge metrics were only weakly correlated to the snow depth, but the relationship did improve when setting edge direction and distance as interaction terms as with Site K for *edge * distance*. *Distance* from edge did not display a nonlinear relationship, as opposed to Site K. The strongest model, *edge*

* *distance* + *concavity*, had an r-squared of 0.35 (RMSE = 13cm). All models had relatively low RMSEs (13 – 16cm) and were statistically significant (p-values < 0.00). Although *distance* had low individual correlation with snow depth, its interaction effect in *distance* * *edge* was a strong improvement over the additive model (r^2 = 0.16 vs. 0.11 respectively).

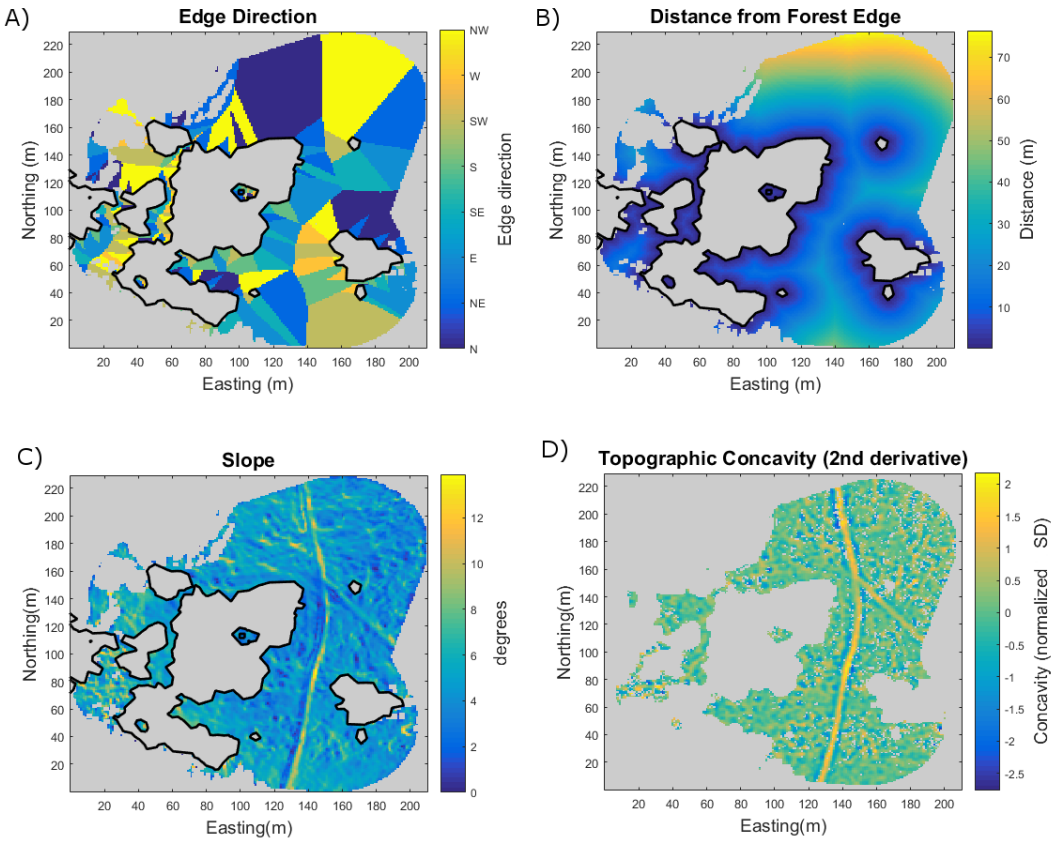

Figure 2.6: Site F selected predictor variables. a) Edge. b) Distance. c) Slope. d) Concavity

Table 2.4. Results from model building process for Site F.

Model						R^2	RMSE	Relative RMSE (%)	P-Value
7	Dist	*	Edge	+	Conc	0.35	0.13	11.0	0
6			Edge	+	Conc	0.28	0.13	11.0	0
5	Dist			+	Conc	0.19	0.14	11.9	0
4					Conc	0.18	0.14	11.9	0
3	Dist	*	Edge			0.16	0.14	11.9	0
2			Edge			0.09	0.15	12.7	0
1	Dist					0.01	0.16	13.6	0

Site O

Site O is on the east side of Grand Mesa, approximately 5km east of the Mid Mesa Met Station. It is similarly sheltered like K, with thick forest on 3 sides and a large, exposed opening facing east, nearly parallel with the predominant wind direction (Figures 2.2C and F). Site O has a significant hill in the southeast corner (Figure 2.7C) strewn with boulders and small dense trees, which abuts a u-shaped forest edge. Snow scans were taken on February 25th, 2017. Mean snow depth was 159cm (SD = 13cm). The strongest predictor variable at Site O was *aspect* with an r^2=0.25 (RMSE = 11cm; Table 2.5). The RMSE of the constant model was 13cm. The next were *concavity* and *edge* with r^2 values of 0.15 and 0.16 respectively (RMSEs of 12cm for both). *Distance* (log-transformed) was not correlated to snow depth (r^2 = 0.01), however when interacted with edge as *edge * distance* the correlation nearly doubled (r^2 = 0.30; RMSE = 11cm) when compared to an additive model (Figure 2.3). Of note too was the interaction between topographical metrics. Independently, *slope* had no correlation (r^2 = 0.00). When interacted with *aspect*, the interaction explained an additional 14% of the variation in

snow depth at the site (*Slope* * *Aspect* $r^2 = 0.39$; RMSE = 10cm). The range of slope values was much greater for Site O than for Sites K and F, with a maximum slope of 31.7º (Table 2.1). Aside from a steep hill in the southeast corner of the site, Site O had similar relief (less than 18°) to the other sites.

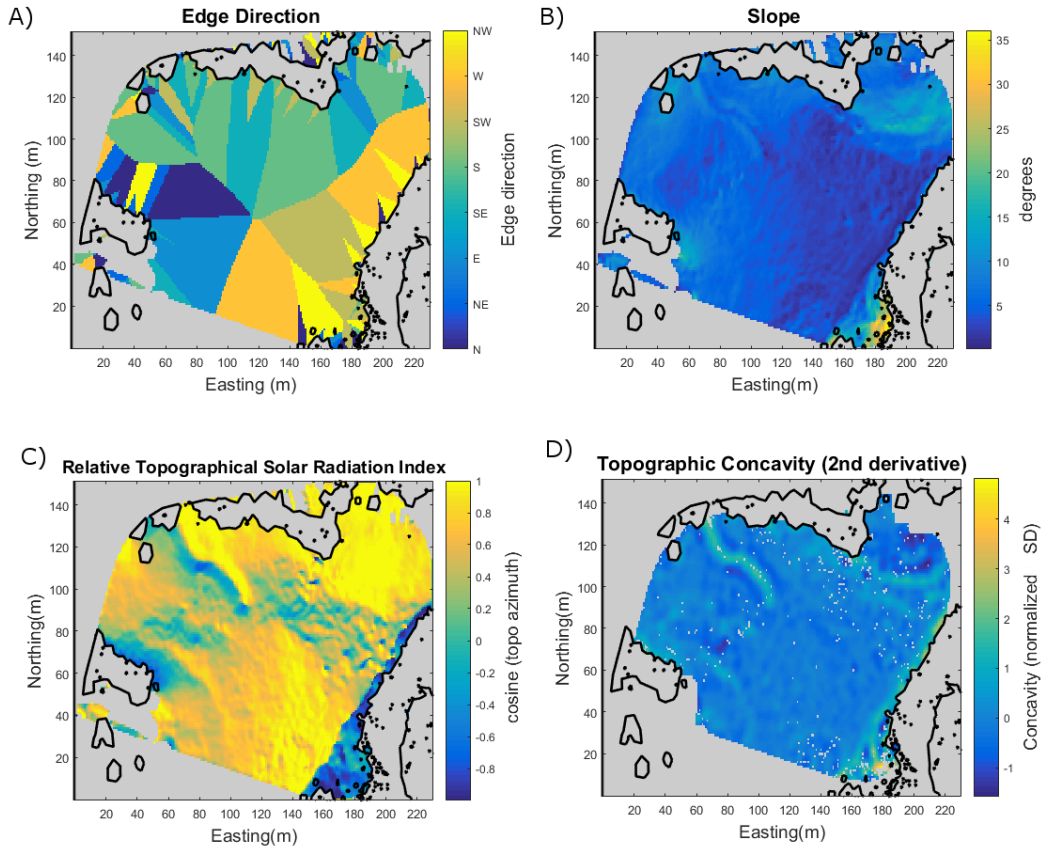

Figure 2.7. Site O selected predictor variables. a) Edge. b) Slope. c) Aspect. d) Concavity.

Table 2.5: Results from model building process for Site O.

Model										R^2	RMSE (m)	Relative RMSE (%)	P-Value
31	Dist_log	*	Edge	+	Slope	*	Asp	*	Conc	0.64	0.08	5.0	0
30	Dist_log	*	Edge	+	Slope	*	Asp			0.55	0.09	5.7	0
29	Dist_log	*	Edge	+			Asp	*	Conc	0.55	0.09	5.7	0
28	Dist_log			+	Slope	*	Asp	*	Conc	054	0.09	5.7	0
27			Edge	+	Slope	*	Asp	*	Conc	0.50	0.09	5.7	0
26	Dist_log	*	Edge	+			Asp			0.46	0.09	5.7	0
25			Edge	+	Slope	*	Asp			0.46	0.09	5.7	0
24	Dist_log		Edge	+	Slope	*			Conc	0.44	0.10	6.3	0
23					Slope	*	Asp	*	Conc	0.44	0.10	6.3	0
22	Dist_log			+	Slope	*	Asp			0.43	0.10	6.3	0
21	Dist_log	*	Edge	+					Conc	0.43	0.10	6.3	0
20	Dist_log	*	Edge	+			Asp	*	Conc	0.42	0.10	6.3	0
19	Dist_log			+			Asp	*	Conc	0.41	0.10	6.3	0
18					Slope	*	Asp			0.39	0.10	6.3	0
17			Edge	+			Asp			0.37	0.10	6.3	0
16							Asp	*	Conc	0.31	0.11	6.9	0
15	Dist_log	*	Edge							0.30	0.11	6.9	0
14	Dist_log	*	Edge	+	Slope					0.30	0.11	6.9	0
13	Dist_log			+			Asp			0.29	0.11	6.9	0
12			Edge	+	Slope	*			Conc	0.29	0.11	6.9	0
11			Edge	+					Conc	0.28	0.11	6.9	0
10							Asp			0.25	0.11	6.9	0
9	Dist_log			+	Slope	*			Conc	0.23	0.11	6.9	0
8	Dist_log			+					Conc	0.22	0.11	6.9	0
7					Slope	*			Conc	0.18	0.12	7.5	0
6			Edge							0.16	0.12	7.5	0
5			Edge	+	Slope					0.16	0.12	7.5	0
4									Conc	0.15	0.12	7.5	0
3	Dist_log									0.01	0.13	8.2	0.01
2	Dist_log			+	Slope					0.01	0.13	8.2	0
1					Slope					0	0.13	8.2	0.10

Discussion

No single metric or model showed consistently good correlation with snow depth across sites. However, the strongest and most parsimonious models always included edge representation, either implicit or explicit. Sites O and K had modest correlation between edge metrics and snow depth ($R^2 = 0.30$ for *edge * distance* at both sites). An implicit representation of edge direction, *asp * slope,* outperformed the explicit *edge * distance* at Site O and aligned with expected wind deposition given the wind direction and forest shape (u-shaped enclosure). Variation in coefficient strength and model correlation at each site depend on the wind regime and forest structure. Spatial variation in snow depth should reflect accumulation and redistribution processes as snow depth scans were taken in February when no melt was observed in snow pit profiles on Grand Mesa.

The rapid, asymptotic increase in snow depth away from the forest edge at Site K (out to approximately 5m) could be due to canopy interception or wind redistribution along forest-related topographical features. The *concavity* and *slope* at Site K, particularly in the southern and southeastern region of the canopy opening, follow the contour of the forest edge (Figures 2.4C and D). There are local depressions in this area bordered by the forest on the south and east, and slight hills to the west and north. This SE corner has deeper snowpack atop these convex features. Wind redistribution may be occurring along topographical features that follow the forest shape, at tens of meters from the forest edge where edge direction is more indiscriminate and overlaps with nearby forest edge directions.

The edge direction metric struggled classifying topological relationships along curved edges and u-shaped enclosures. This is evident at Site F. The large drifts on the

north edges of the two patches were almost exclusively within N and NW edge directions. Model intercepts (coefficients) for these edges were the largest at the site (129 and 122cm for N and NW; mean intercept for all edges = 115cm; Table A.2). However, the other clear snow drift, within the u-shaped enclosure midway down the eastern edge of the large patch is composed of nearly every edge direction. These drifts are consistent with the NW-SE prevailing winds recorded at the Mid Mesa meteorological station, the closest weather station to Site F on Grand Mesa.

Site O is within 5km distance of the Mid Mesa meteorological tower, and is situated in a similar forest type and topography. Mid Mesa records the predominant wind direction as nearly symmetrical along the SE-NW axis, with more frequent heavier winds to the NW (Figure 2.8). Winds blowing NW account for 36% of total wind distribution vs 25% for SE blowing wind. Site O has significant relief (hills), so direct comparisons to the wind dynamics at Sites K and F are nuanced. The forest enclosure along this SE hill acts as a snow fence (Hiemstra et al., 2002), wherein blowing snow has no escape route to enable a flow separation zone in which to deposit snow. Snow is deepest along this hill (Figure 2.2F), however a gentler, but still relatively steep hill in the NE corner of the site shows the opposite effect (less than site average snow depth). This demonstrates why slope independently of a wind or terrain parameterization has an ambiguous relationship to snow redistribution, and why slope had no correlation to snow depth (r^2=0.00) at this site.

As with Site O, the edge direction calculation is not ideal because the forest edge delineation workflow incorporates short edge segments from high frequency changes, producing large ranges of edge directions over short distances, not representative of the

predominant direction in u-shaped enclosures and jagged forest edges. *Aspect* was more successful than *edge* at Site O (r^2 = 0.25 and 0.16 respectively) because the slope was steep enough to produce only a small range of zenith measurements (aspect) under the large snow drift in the SE corner that aligned with the predominantly west-northwest facing forest edge.

Each of these sites represent areas with distinct physiographic characteristics along Grand Mesa and this is borne out in the range of topographic metric values (Table 2.1) and modelling results between sites. Site K is just on the edge of the shrub-steppe to forest ecotone about midway across the Grand Mesa Study Area; Site F is situated in an intermediate forest density area; Site O, 22km to the east, is in a dense continuous forest among rolling hills and small lake depressions. As has been reported with similar approaches relating snow depth to static topographical parameters that ignore wind redistribution, much of the variation will go unexplained. This analysis would benefit from a dataset with a larger extent such as airborne lidar to capture the range in topography and forest configurations, or in the case of this data, the gradient between these sites. This would enable a large sample size of forest patches and edges, and the testing of terrain parameterizations designed to model wind deposition from topography.

Distance in *edge * distance* reinforced previous work constraining forest edge wind deposition to specific distance ranges away from the forest edge, and showed that edges have significantly different snow distributions at close ranges depending on their direction. The r^2 went up 13%, 37% and 39% (0.26 to 0.30, 0.10 to 0.16, and 0.17 to 0.28) for Sites K, F and O respectively from the additive *edge + distance* to *edge * distance* models. The improvement in correlation from adjusting the intercept and slope

coefficients in the linear regression for each edge direction in all cases was an improvement over simply varying the intercept between edge directions. Not all edge direction adjustments were statistically significant, however the intercepts in particular had ranges of 15cm (136 – 151cm) and 19cm (103 – 122cm) at Sites K and F respectively (Tables A.1 and A.2). Edges could be aggregated into cardinal directions or custom ranges aligning optimally with site or region specific prevailing wind directions.

Implicit edge representations may also be worth testing at sites with meadow forest patch complexes such as Grand Mesa with similar snow drifts along or at the base of slopes. Edge direction, as represented by the implicit edge representation, *aspect * slope,* had modest correlation at Site O and outperformed the best explicit edge model, *edge * direction. Aspect * slope* was the best performing two metric model at any of the sites. For Site O, the snow drifting in the SE corner was seemingly driven by a relatively steep hill partially-enclosed by a forest edge oriented perpendicular to the predominant wind direction. *Aspect* and *slope* (Figure 2.7C and B) in *aspect * slope* are able to isolate the relatively deep snow drift on the hill below the snow fence and more accurately classify edge direction than the explicit *edge* or *edge * distance* models. In both the implicit and explicit edge models, metrics with no correlation to snow depth at a particular site added significant correlation to models as interaction terms.

Static topographical representations (global parameters) of flow confluence zones in respect to wind flow are commonly used to predict snow distribution (Williams et al., 2009). Edge direction and distance has primarily been used to understand the energy balance inside forest gaps (Webster et al., 2017), and more recently to identify differential ablation and accumulation along forest edges (Currier and Lundquist, in

press). In this study they were tested as proxies for wind redistribution along forest edges. Aside from Site O, there was mostly weak to moderate correlation, even with the models that used all available metrics. Site O had relatively strong correlation, with an $r^2 = 0.64$ using common topographic variables and the edge metrics. This may be because the spatial variation is distributed evenly throughout Sites K and F, as opposed to the localized snow drift at Site O. A more sophisticated edge direction metric that differentiates exposed edges from u-shaped alcoves which can also incorporate the predominant edge direction (disregard small-scale changes) may be capable of modelling wind distribution patterns along forest edges. More precise metrics applied to a larger area with more forest edge and gap samples may prove useful in an approach incorporating edge direction metrics.

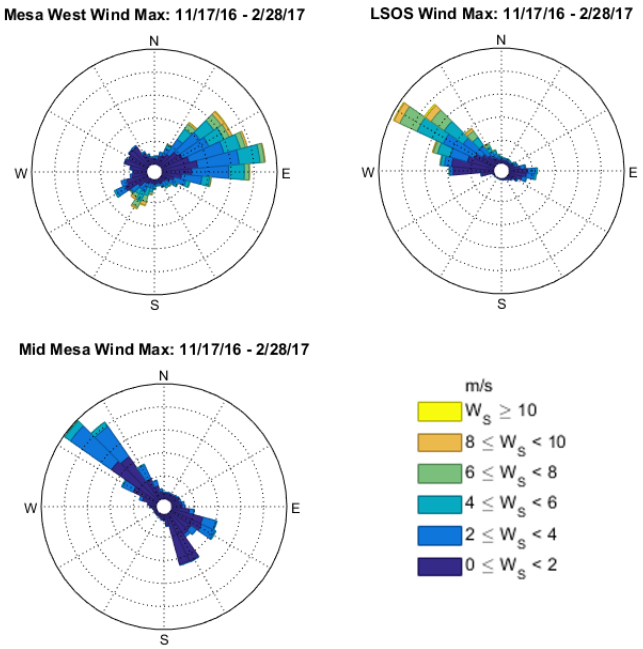

Figure 2.8: Wind direction and frequency at three meteorological towers on Grand Mesa.

Conclusion

Three TLS plots representing a range of forest cover and wind conditions from the 2016-2017 SnowEx field campaign at Grand Mesa, CO, were used to test the relationship between simple proxies for wind deposition in open areas along forest edges prior to the onset of the snowmelt period. Correlation was modest at sites with evenly-distributed snow depth and minimal slope, and strong at the site with larger, concentrated snow depth variation and a steeper slope. The strongest and most parsimonious models always included either implicit or explicit edge representation. Site O, a site with a large, concentrated snow drift showed the best overall correlation at $r^2 = 0.64$. Log-transformed distance (*distance)* alone explained 22% of the variation at Site K, and *edge* 18% at Site O. Nearest edge direction and log-transformed distance from edge (*edge * distance*) had an $r^2 = 0.30$ at Sites O and K, indicating significant differences in snow depth based on edge direction, distance from edge or both, and a non-linear change in snow depth away from the forest edge. At Site O, the implicit measure of edge direction and distance, *aspect * slope,* had an $r^2 = 0.39$, outperforming the explicit edge representation, *edge * distance*. This alternative edge representation may be useful at windy, hilly sites.

References

Currier, W. R., & Lundquist, J. D. (in press). Snow depth variability at the forest edge in multiple climates in the western United States. *Water Resources Research.*

Deems, J. S., S. R. Fassnacht, and K. J. Elder (2006), Fractal distribution of snow depth from LIDAR data, J. *Hydrometeor*., 7(2), 285 - 297.

Elder K., Dozier, J. and J. Michaelsen (1991), Snow Accumlation and Distribution in an Alpine Watershed, *Water Resour. Res.* 27(7), 1541-1552.

Hall, D. K., Riggs, G. A., & Salomonson, V. V. (1995). Development of methods for mapping global snow cover using moderate resolution imaging spectroradiometer data. *Remote sensing of Environment*, 54(2), 127-140.

Hiemstra, C. A., Liston, G. E., & Reiners, W. A. (2002). Snow redistribution by wind and interactions with vegetation at upper treeline in the Medicine Bow Mountains, Wyoming, USA. *Arctic, Antarctic, and Alpine Research*, 34(3), 262-273.

Jähne, B., Haussecker, H., & Geissler, P. (Eds.). (1999). *Handbook of computer vision and applications* (Vol. 2, pp. 118). San Diego: Academic press.

Marks, D., Domingo, J., Susong, D., Link, T., & Garen, D. (1999). A spatially distributed energy balance snowmelt model for application in mountain basins. *Hydrological Processes*, 13(12-13), 1935-1959.

Shrivakshan, G. T., & Chandrasekar, C. (2012). A comparison of various edge detection techniques used in image processing. *International Journal of Computer Science Issues (IJCSI)*, 9(5), 269.

Streutker D., and N. Glenn. (2006). LiDAR measurement of sagebrush steppe vegetation heights. *Remote Sensing of Environment*, 102, 135-145.

Trujillo, E., Ramírez, J. A., & Elder, K. J. (2007). Topographic, meteorologic, and canopy controls on the scaling characteristics of the spatial distribution of snow depth fields. *Water Resources Research*, 43(7).

Webster, C., Rutter, N., & Jonas, T. (2017). Improving representation of canopy temperatures for modeling subcanopy incoming longwave radiation to the snow surface. *Journal of Geophysical Research: Atmospheres*, 122(17), 9154-9172.

Williams, C. J., McNamara, J. P., & Chandler, D. G. (2009). Controls on the temporal and spatial variability of soil moisture in a mountainous landscape: the signature of snow and complex terrain. *Hydrology and Earth System Sciences*, 13(7), 1325-1336.

Winstral A., Elder, K., and RE Davis (2002), Spatial snow modelling of wind-redistributed snow using terrain-based parameters, *Journal of Hydrometeorology*, 3(5), 524-538.

Winstral, A., & Marks, D. (2002). Simulating wind fields and snow redistribution using terrain-based parameters to model snow accumulation and melt over a semi-arid mountain catchment. *Hydrological Processes*, 16(18), 3585-3603.

CORRELATING THE SPATIAL DISTRIBUTION OF SNOW DEPTH UNDER VARIOUS FOREST COVER TYPES AND SCALE REPRESENTATIONS

Introduction

The incorporation of remotely-sensed data into snow process research has been recognized for decades by snow hydrologists as crucial to understanding large process scales (Rango, 1993). Various airborne sensors have successfully captured watershed-scale and continent-scale data to this effect (Painter et al., 2016; Hall et al., 1995), but remote sensing retrievals in forested regions are confounded by forest cover (Deems et al., 2013). Lidar however is capable of penetrating relatively dense forest to retrieve spatially-distributed snow depth measurements. Challenges with lidar exist, particularly accessibility due to cost and extent of coverage. There are no mid-latitude orbiting satellites designed to monitor snow hydrology with lidar (though IceSAT-2 was recently launched and its photon counting technology will be used for cryosphere observations over relatively coarse spatial and temporal scales, and was designed for monitoring ice sheets and glaciers in the polar regions, not seasonal snow). Watersheds in California, including the Toulomne Basin, are one of few examples worldwide where lidar is used operationally to forecast water supply in a snow dominated watershed (Hedrick et al., 2018). As a result, multi-year subcanopy snow observations on large, regional scales are limited.

The recognition of the knowledge gap in subcanopy regions by the snow science community and NASA comprises much of the motivation for the SnowEx mission, and

this research. Forests are characterized in the snow literature qualitatively (“gap”, “thinned”, “old growth” [Dickerson-Lange et al., 2015]; “uniform”, “discontinuous”, “dense” [Pomeroy et al., 2009]), yet translating this into quantifiable measurements depends on the application and data source. Unlike optical imagery and photogrammetrically-derived point clouds, lidar can reach the forest floor, allowing three dimensional forest structure effects on snow accumulation and ablation to be studied at much finer scales and accuracies than current optical-based satellite canopy cover products (National Land Cover Database 2011 United States Forest Service tree canopy analytical). Measures of canopy cover (canopy closure or sky view fraction [SVF]) and cross-sectional foliar density (leaf area index) are the main canopy proxies in interception models (Hedstrom et al., 1998). SVF is essentially the proportion of unobstructed sky from a given spot on the ground facing upward (Matzarakis and Matuschek, 2011). Radiation is calculated using SVF to partition sky, snow and canopy longwave emissions, as well as direct solar radiation. Forest cover metrics can be incorporated into watershed and regional scale models by relating canopy cover distributions to fractional melt patterns using snow depletion curves (Dickerson-Lange, et al., 2015; Luce et al., 1999), as pixel-level tuning with binary or weighted (Hedrick et al., 2018) snow depth correction factors, or a hybridized fashion that adjusts hydrological outputs differently in open areas based on their size and relationship to the surrounding forest (Seyednasrollah & Kumar, 2014). In either case, the model scale must be optimized to the process scale (Bloschl et al., 2001) in representing snow processes.

Snow mass and energy balance models can significantly underestimate net snow water input in forested areas when pixel resolution is too coarse to capture the high

frequency variation in depth present along the edge and under the canopy (Broxton et al., 2015). Given the unique gradient in forest density, structure and configuration at Grand Mesa, units of analysis in this study will be both at the pixel scale, and at the patch level. The concept of patches has been used in landscape ecology to investigate relationships between ecological phenomena or processes and patterns of forest cover (McGarigal et al., 2002). Tree stands of similar environmental states with distinct boundaries can be aggregated into larger units, or patches. The conditions that enable various forest configurations and patch properties can be attributed to coupled environmental, geologic, geomorphic and physiographic processes including wind patterns and soil moisture and snow distribution (Malanson et al., 2007). Forest shape and configuration is not only a result of these processes, but part of a feedback loop which equilibrates physiographic landscape attributes with snow and moisture distribution patterns. Ribbon forests, a common forest type within the timberline to alpine ecotone in the Rocky Mountains, illustrate this concept. Characterized by rows of thin, strip-like forest ribbons oriented perpendicular to the prevailing winds (Smith et al., 2003), ribbon forests are a first order result of exposure to heavy winds and subsequent snow deposition processes which promote krummholz tree forms on windward exposures, and upright forests on sheltered, leeward sides (Malanson et al., 2007). A gradation from sparse ribbon forests to more typical, mature forests expands upslope as wind turbulence is impeded by progressively denser forests. Grand Mesa exhibits a similar forest cover progression, albeit not a ribbon forest.

The impetus for this study is to further contribute to the understanding of forest canopy – snow interactions by exploring how vertical forest canopy structure differences

affect snow depth distribution during the snow accumulation period. Various spatial scales will be investigated to relate evidence of scale-dependency to forest type density and shape. We hypothesize that subcanopy snow depth will be best correlated to canopy metrics at spatial resolutions within the correlation length of the canopy. As forest density, tree spacing and distribution drive patterns in spatial variation of the canopy, it follows that a spatial resolution less than the correlation length of the canopy yet small enough to detect small changes in that range, should yield the best correlation if snow depth variation is due to canopy interception at the tree level.

Methods

Evaluating Spatial Resolution Limits

We wanted to leverage the inherently fine spatial capabilities of TLS data by using the finest spatial resolution possible, which in this case was limited by the distribution of ground returns. Ground point distribution in the fall scans was effectively thinned to the frequency of the surface roughness by the ground classification algorithm. Therefore, ground and consequently snow depth, was the limiting factor in upsampling to smaller snow depth grid cells.

To determine the lowest acceptable spatial resolution of our data, progressively smaller snow depth maps were created from the point cloud and loss in coverage was compared. Our main consideration was not the area lost, but representation lost, i.e. "coverage". Each snow depth pixel requires a pair of overlapping ground (fall) and snow surface (winter) pixels or points. For instance, upsampling from a $1m^2$ pixel into four $0.5m^2$ pixels can result in either zero, one, two, three, or four overlapping, paired fall/winter pixels (0, 25, 50, 75 or 100% coverage). If at least one of the four resampled

0.5m pixels contains overlapping ground and snow points, then a snow depth pixel can be created, and this is considered “coverage”. However, if the larger pixel did not contain a single smaller pixel, then the upsampling resulted in a loss in coverage at that pixel (Figure 3.1). This workflow was run at progressively smaller pixel sizes: 0.5m^2, 0.25m^2, and 0.10m^2. Percent coverage was calculated for each resampled size at Sites K and N as the percent of original 1m^2 snow depth pixels with coverage after upsampling. As an example, coverage from Site K for the 0.5m^2 resolution is presented in Figure 3.2.

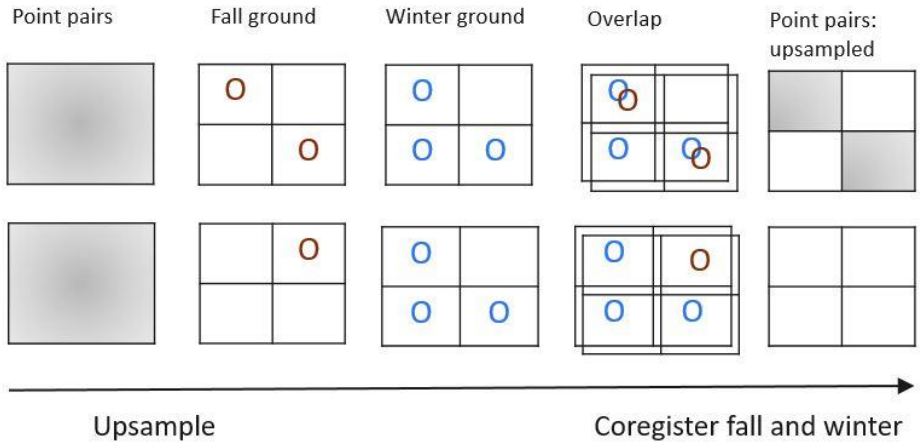

Figure 3.1. Two examples of coverage. Red circle indicates ground points in the fall. Blue are ground points in the winter (snow surface). Shaded gray are pixels with point pairs where snow depth can be calculated. Upsampled with resultant coverage (upper row); upsampled with no coverage (lower row).

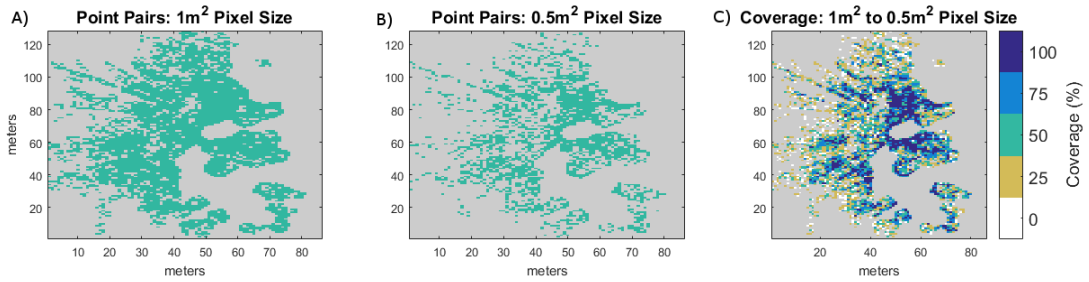

Figure 3.2. Coverage in canopy. A) 1m2 point pairs (i.e. overlapping fall and winter points where snow depth can be calculated). B) 0.5m2 point pair. C) Percent Coverage: Percent 0.5m2 point pairs contained within 1m2 point pairs.

Delineating Individual Trees

Individual tree locations and heights were found using a local maxima (LM) algorithm. LM algorithms are a ubiquitous method for single-tree identification in forest inventory surveys, and in multiple comparison tests are top-performers in optimizing commission and omission errors (Vauhokenen et al., 2011, Eysn et al. 2015) and identifying dominant and subdominant trees in airborne lidar tree surveys. Multiple studies have found that smoothing the canopy height model prior to the LM run is the most critical part (Solberg et al., 2006); more so than the point density of the data or algorithm selection (Vauhkonen et al., 2011). For this dataset, the canopy height model (CHM) was interpolated from the cleaned and classified point cloud at a 0.5m resolution. Maximum height within each cell was assigned to each cell. Gaussian and median filters are commonly used to remove noise from the raw CHM (Solberg et al., 2006; Persson et al., 2002). This CHM was filtered using a 2 dimensional 3X3 median filter to remove noise. Our CHM size was 0.5m. CHM sizes of 0.25m and 1m were also tried along with all local maxima window sizes from 1 to 7 pixels. Best results were found with the 0.5m CHM and two pixel search window for the LM process. Parameters were optimized using Site K as validation both visually and with measures of classification accuracy, commission and omission.

The above referenced literature and discussion refers to airborne lidar, whereas this dataset is TLS. As point density has not been found to significantly impact the results of raster-based tree identification, it follows that these algorithms are effective with hyper dense TLS point clouds. Site K was used for validation. Tree locations were manually identified from the point cloud for the entire site. Manually located tree tops were

compared to the results from the automatically identified trees to assess accuracy (Figure 3.3). For this method at Site K the commission rate was 8% and the omission rate was 17% (Table 3.1). For comparison, tree detection (matching) rates for single layer and multi-layer coniferous forests using state-of-the-art extraction methods (LM or otherwise) in an alpine environment was 60% and 35% respectively (Eysn et al., 2015) for airborne lidar. For the dominant height classes, tree matching rates regularly achieve 80% range in the referenced studies. Based off the high accuracy of this automated tree detection method found at Site K, and the cited success in identifying larger, dominant trees, we used this method to identify trees in the remaining sites (Sites F, O and N). The mean height of detected and undetected trees was 18.8m and 15.8m respectively. Undetected trees were generally in close proximity to larger trees, and had overlapping, sometimes indeterminate canopies.

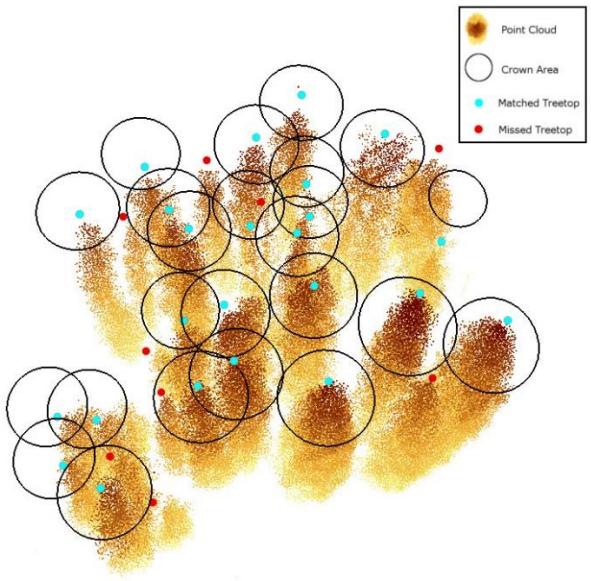

Figure 3.3: Sample patch of automated tree top extraction results. All dots are tree tops manually identified in the point cloud (true trees). Black circles are modelled tree crown canopies based off measured height values for true trees. Red dots are true tree tops

Table 3.1: Classification assessment from individual tree identification

Measure	Accuracy (%)
Commission	8
Omission	17

Vegetation Metrics: Canopy Structure Models

Multiple vegetation metrics were calculated at all sites. Variables directly calculated from the point cloud were created using BCAL Lidar Tools. These variables are used as proxies for forest canopy cover. There are 35 metrics which can be classified into two categories: vertical distribution metrics and point classification metrics (Appendix A.4; Dhakal, 2016). To calculate these metrics, the point cloud is overlaid with discrete cells. Lidar points contained within each grid cell boundary are used to calculate each of the 35 metrics at each respective grid cell, yielding a continuous raster with values for each of the 35 metrics. For example, mean is the mean height of all classified canopy points within a pixel. Metrics include basic statistical descriptors of distribution (minimum, maximum, range, etc.), moments (mean, variance, skewness and kurtosis), the interquartile range and frequency of points within a defined range (i.e. 5m-10m), height values at specified percentiles (i.e. 5^{th}) as well as other variables capable of differentiating vertical height distribution nuances (i.e. median absolute deviation from median height). Within the vertical distribution category there was also a functional covariate of vegetation canopy distribution called foliar height diversity (FHD) (MacArthur and MacArthur., 1961). The second category of BCAL metrics, point classification metrics, convey both the actual and relative number of ground and canopy points within each cell. Values of 0.15m and 0.5m ground and canopy thresholds were used respectively as parameters to calculate ‘Vegetation Metrics’ in BCAL Lidar Tools.

The ‘vertical bin spacing’ parameter used to calculate FHD was set to match the horizontal spacing (i.e. 1m for $1m^2$ and 3m for the $3m^2$ grid size).

Scales of Analysis

Correlation analysis was performed at both the pixel and patch scales. For the pixel scale, multiple spatial resolutions were examined for scale-dependent relationships between the forest canopy and snow depth. The patch scale approach delineated large forest patches as objects and compared bulk properties of the patch to those of the snow depth.

Pixel-Level Analysis

Up to four spatial resolutions were used: 0.25, 0.5, 1 and $3m^2$. Snow depth was regressed against each of the 35 BCAL metrics at each pixel location, and a linear model was fit based on r^2 values in order to rank the best individual predictors of snow depth. As will be discussed later, metrics were clustered based on their coefficients of covariance (Figure A.1), and at a minimum, one metric from each group will be presented and discussed.

Patch-Level Analysis

In contrast to pixel-level analysis, patch-level analysis aggregates the forest into homogenous, distinct patches. At each site, patches were manually delineated using the canopy height model as a guide, along with optical satellite imagery (National Agricultural Imagery Program, NAIP) to visualize the smaller TLS sites in the larger context of the landscape. Polygon boundaries were drawn around large forest clusters at each site. All sites but one (Site A) had two patches, for a total of seven forest patches across the four sites (Figures 3.4, 3.5, 3.6). Patches were easily identifiable for all but Site

N. This site was logged in the 1950's and now is covered with second-growth pine with evenly distributed individual trees as opposed to distinctive patches (Figure 3.4). Due to this, patches were delineated using subtle edge breaks between adjoining patches. The western patch at Site K involved some subjectivity as one smaller tree cluster was detached but nestled on the edge of the patch. The patch was traced excluding this cluster as the perspective from the NAIP image revealed that the majority of this patch's border was continuous, and without small aggregated clusters. Site A was situated on the edge of a single, isolated patch. As such, Site A only produced one patch for analysis. There was a slight inroad into the canopy ~20m from the furthest snowcover extent where the canopy point cloud was noticeably thinner, which was used to demarcate the eastern edge of the patch. The limited spatial extent of TLS, particularly in the forest, resulted in the point cloud only covering a portion of the larger patches on which they were situated. Therefore, the patches we used are samples of and assumed to be representative of larger patches. The exception is the smaller, eastern patch at Site F.

At each patch, pixels were averaged, yielding one mean value per metric, per patch. Pixels without canopy cover were assigned zero, and included in the average. In addition to the BCAL metrics, statistics from delineated trees were used. These included: tree density (stems per acre), total number of trees, average tree height and standard deviation of tree height per patch. In contrast to the BCAL metrics, these are not patch averages of pixel values, they are direct measures of the population of trees identified within each patch. Elevation of the patch was also analyzed for correlation. Patch means accounted for fractional cover as open pixels were assigned zero, lumped in and averaged with the canopy pixel. This in effect accounted for fractional canopy cover within each

patch. As an additional, basic measure, fractional cover was also created. Fractional cover was simply the number of pixels within the patch with canopy cover over the total number of pixels, from 0 to 100%.

Open areas without canopy cover (polygons) were also delineated to compare with forested areas. Each site had one representative open area. The size of each open polygon was well within one order of magnitude of the canopy patches, and in some cases, larger. Roads and trails were avoided, as well as snow drifts and scour areas. The snow distribution from these open areas were compared with snow under the canopy. Specifically, the ratio of canopy:open was calculated using the average snow depth from both (or one at Site A) canopy patches and the average from the open area.

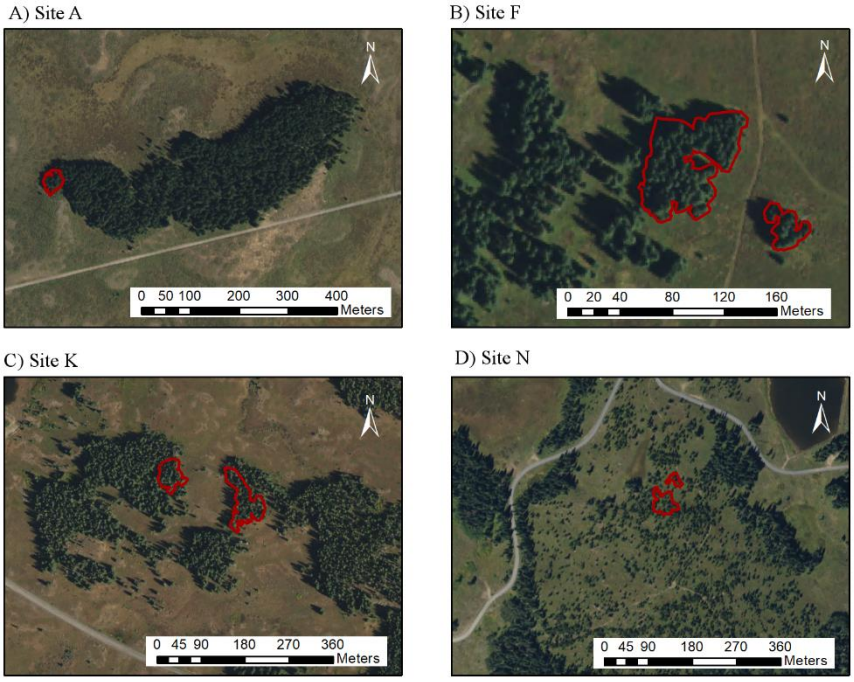

Figure 3.4: NAIP images of sites with patch boundaries outlined (red). Site names labeled on figure.

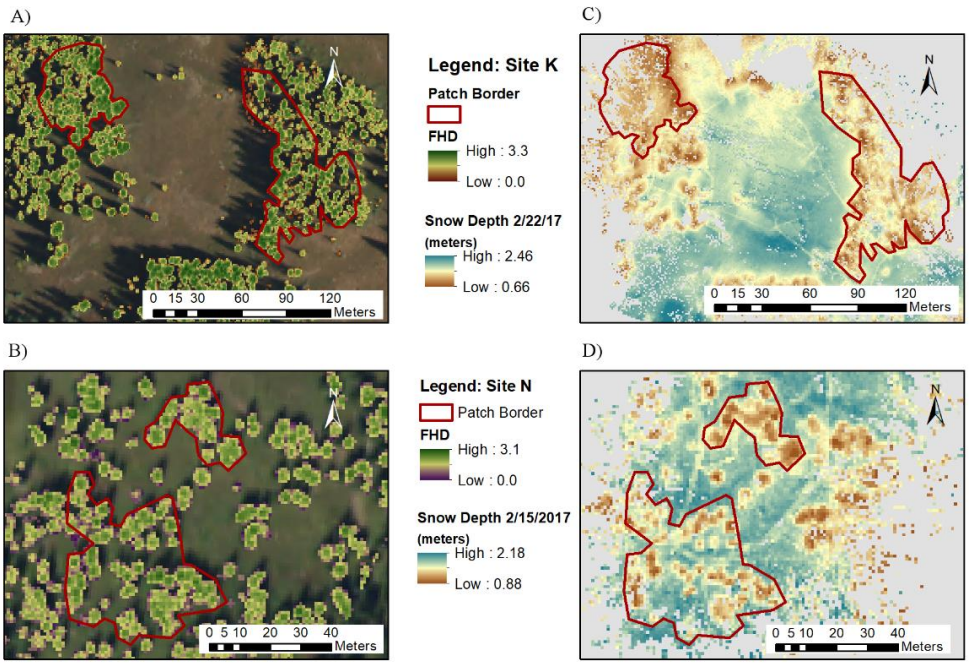

Figure 3.5: Sites K and N foliar height diversity (FHD) and snow depth with patch border (red). A) Site K with FHD metric displayed. B) Site N with FHD metric. C) Site K snow depth. D) Site N snow depth

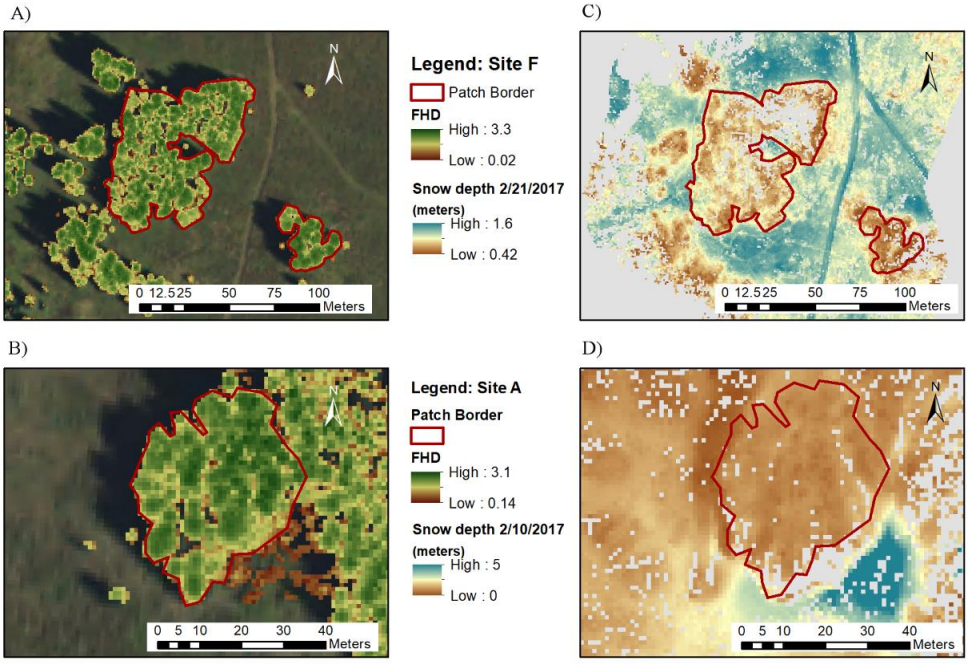

Figure 3.6: Sites F and A foliar height diversity (FHD) and snow depth with patch border (red). A) Site F with FHD metric displayed. B) Site A with FHD metric. C) Site F snow depth. D) Site A snow depth

Variable Assessment and Workflow

Each of the variables was regressed versus snow depth in a linear regression. Many of the variables, particularly those in the heavily represented vertical distribution (n=30) category were highly correlated. A correlation matrix was created (Figure 3.4), and 40% of all variable pairings had correlation coefficients of a magnitude greater than 0.8. Variables were distilled to reduce data and illustrate the most pertinent relationships to the narrative of our hypothesis. A general ruleset was used to thin variables to be used in further discussion. This included: Variables with $r^2 < 0.57$ were not shown (due to an abrupt threshold where the next highest correlation was $r^2=0.44$) and only one variable from groupings of highly correlated variables were shown. Exceptions are explained below. 16 of the 45 variables had $r^2 > 0.5$. Each of the three categories (vertical distribution, points and trees) had at least one variable with an $r^2>0.57$. Correlation between variables was visually assessed using the correlation matrix, and groups of correlated metrics were noted. To minimize redundant information, only one variable from each group was presented in graphical form. Despite being highly correlated to maximum canopy height (*max*), standard deviation (*std*) and mean height (*mean*) are shown as they are common statistics, and are relevant for comparisons. From 45 variables, seven variables are displayed and discussed in the results. *Elevation*, the one miscellaneous variable, or site property, was not shown but had an $r^2 = 0.30$.

Geostatistical Analysis at Patches

Experimental variograms were made for each patch for both the snow depth and canopy. *Max* was used as the metric in the vegetation variogram. A spherical model was fit to each of the variograms using R.1.414 (R Core Team, 2017) with the package gstat

(Pebesma, E.J., 2018) using the default settings (least squares). Lag spacing varied by patch (~0.25m – 0.5m); patches with short ranges were given shorter lag spacings to provide more accurate model fit. Parameters from the spherical model fits included range and sill. The uncertainty of model fit was assessed using a randomly sampled 75% of the data for 1,000 Monte Carlo simulations (with replacement) for each patch. Uncertainty was assessed as the standard deviation of the model parameter estimates of the 1,000 Monte Carlo simulations.

Results

Pixel-Scale

We found that the $25cm^2$ pixel size was the finest achievable resolution at our sites. Unacceptable coverage at $0.1m^2$ resolution, a large drop in coverage from $0.25m^2$ to $0.1m^2$, and overall sparse distribution of pixels at Sites K and N limited our resolution to the $0.25m^2$ size. At the $0.1m^2$ spatial resolution the percent coverage was 55 and 68% for Sites K and N respectively (Table 3.2). In other words, Site N had only 68% representation of the original ~9,700 $1m^2$ pixels by at least one of the $0.1m^2$ pixels. At Site K, there was only 55% coverage from an original ~ 9,900 $1m^2$ pixels. Progressively smaller resolutions were analyzed at each site until correlation was worse or stagnated.

Table 3.2: Change in coverage from upsizing various pixel sizes at Sites N and K.

Comparison	Site K Coverage (%)	Site N Coverage (%)
3m → 1m	93	96
1m → 0.5m	95	94
1m → 0.25m	76	85
1m → 0.1m	55	68

Two of our sites showed weak to no correlation with any spatial resolution. Site K had moderate correlation which can be ascertained both from the r^2 value and the

scatterplot of Depth vs. Max (Figure 3.7). Site K showed slight improvement at the larger $3m^2$ spatial resolution compared to $1m^2$. Snow distribution at Site N had relatively strong correlation with multiple lidar metrics, with correlation progressively increasing, and then peaking at the $50cm^2$ pixel size. Correlation at the $25cm^2$ decreased slightly.

Site A showed no correlation between any of the metrics and snow depth at any pixel size, with the best correlation being $r^2 = 0.05$ at FHD above ground (*FHD_ab_grd*) for the $3m^2$ resolution. Site F had very weak correlation at best with $r^2 = 0.16$ for *FHD_ab_grd* at $1m^2$ resolution. At $3m^2$ resolution this same metric performed the best, but at a much lower $r^2 = 0.06$. Site K also had weak correlation, but better than Sites A and F. The $3m^2$ resolution showed slightly better correlation than the $1m^2$ (Average of all metrics $r^2 = 0.12$ and $r^2 = 0.10$ for $3m^2$ and $1m^2$ respectively). *Max* and 95th percentile (*per_95th*) both had an r^2 of 0.27. Site N showed the best correlation to canopy metrics, and also the greatest scale-dependency (Average of all metrics $r^2 = 0.10$ and 0.18 for $3m^2$ and $0.5m^2$, respectively). At the $0.5m^2$ pixel size, correlations were relatively high (r^2 values of: *max* = 0.51, per_95th = 0.43 and *FHD_all* = 0.42). While the difference in the average r^2 was only 0.08 between the two cell sizes, the greatest r^2 for the $3m^2$ was 0.24 (*max*) compared with 0.51 (*max*) using the $0.5m^2$ cell size.

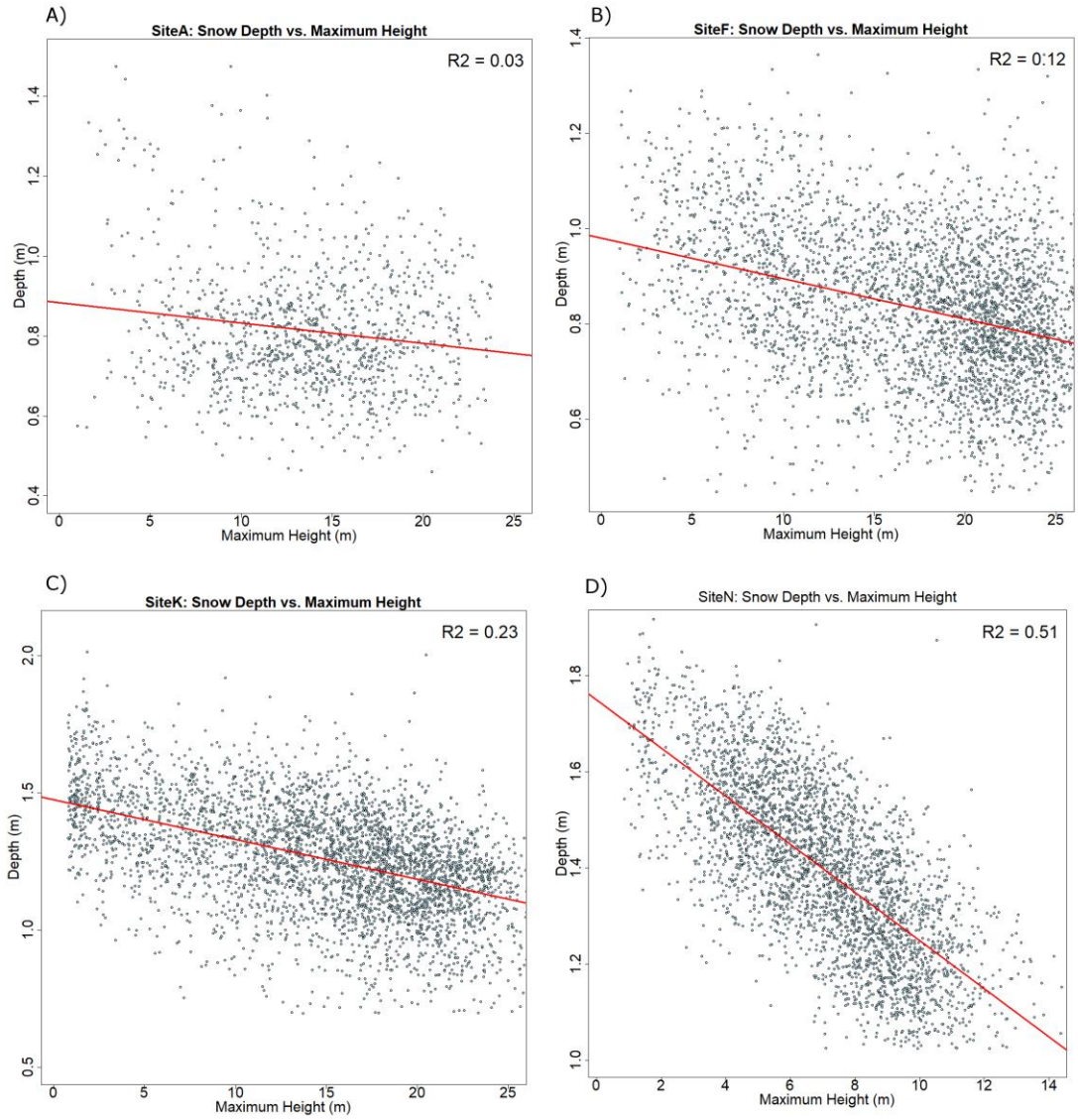

Figure 3.7: Pixel-level correlation at each site. A) Site A. B) Site F. C) Site K. D) Site N (Note: scales differ)

Patch-Scale

Patch averaged statistics had substantially higher correlation to snow depth than even the best pixel-scale relationships. *FHD_ab_grd* had the highest correlation at 0.94 (Figure 3.8a). Basic canopy distribution statistics like *max*, interquartile range (*intrqrtle*) and *Std* were all at or above 0.75 (0.78, 0.76 and 0.75, respectively). Other quartiles also performed well, with progressively better correlation in the higher quarter ranges.

per_95th, *per_90th*, *per_75th*, *per_25th*, *per_10th* and *per_5th* were 0.69, 0.66, 0.61, 0.44, 0.32 and 0.26, respectively. Note that the 50th percentile (*per_50th*) output was excluded due to miscalculation issues with the BCAL software. Of note too was the 0.62 r^2 for *height_avg*, which is the average height identified trees within each patch (Table A.5). Site K for instance had average tree heights of 21.2m (n=131 trees) and 16.6m (n=180 trees) for the west and east patch, respectively. The standard deviation of identified trees per patch (*Height_std)* was 0.22; *Tree count* and *tree density* had no relationship to snow depth (r^2 =0). Elevation also had no correlation (r^2=0.03). Select results are shown in Figure 3.9. Site A did not have statistics from identified trees as we found the automated delineation method insufficient, and manual delineation impossible. The broad shape of trees in the upper canopy led to layering with the lower canopy. This made identifying lower canopy trees suspect. Tightly clustered trees were also indiscernible in many instances.

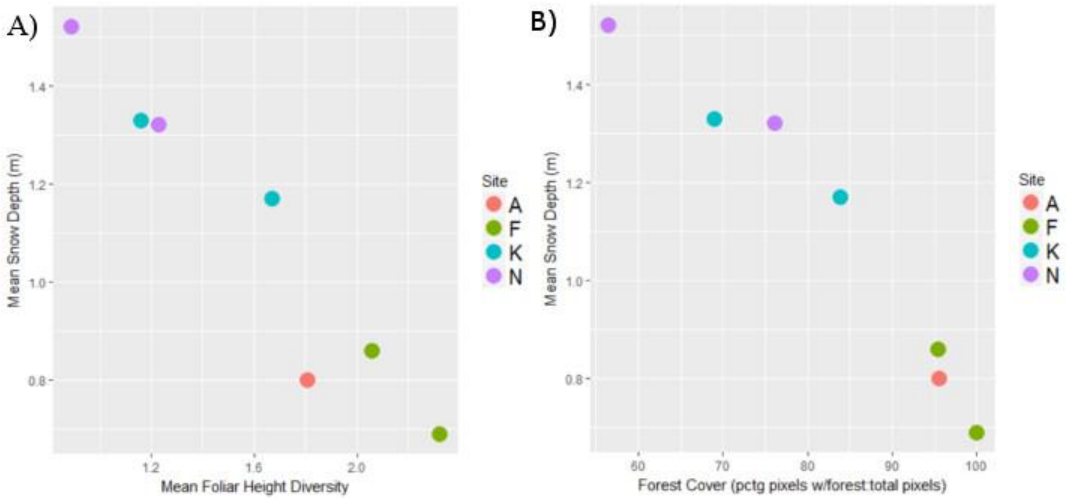

Figure 3.8: Snow depth vs. A) foliar height diversity (FHD_ab_grd) and B) fractional cover

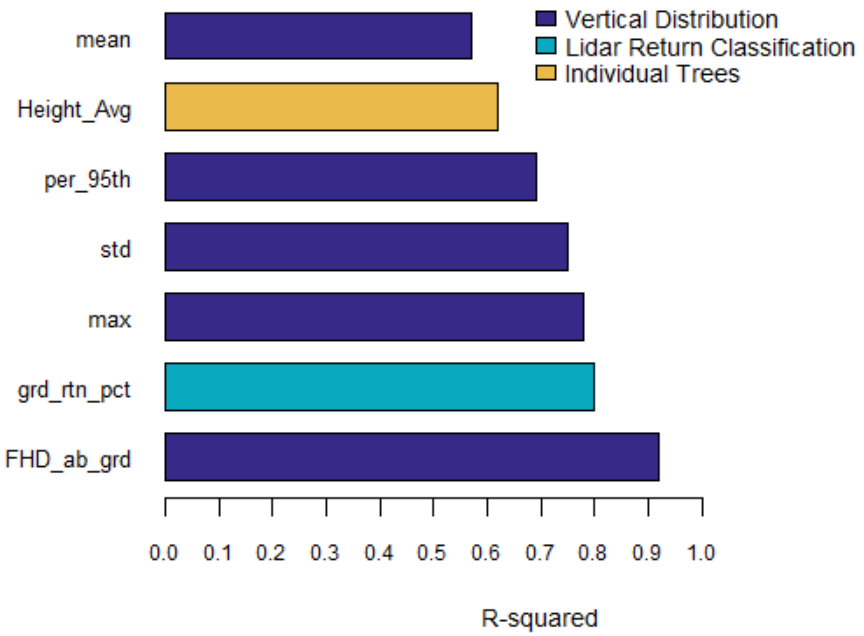

Figure 3.9: Regression results from patch analysis showing a subsample of metrics. Seven of the 45 patch properties tested.

Variogram Analysis

All sites but Site A had clearly defined sills for both the snow depth and *max* variograms. Variogram shapes matched well between the canopy and snow (Figures 3.10 and 3.11), and the range values from model fits were similar between the canopy and snow for most sites. At six of the seven patches, the canopy range was larger than the snow range. Site N had the shortest ranges (3m), and Site F, the largest range (8m).

Table 3.3: Parameters from spherical variogram models. Canopy is max and Snow is snow depth.

Site	Canopy - Range (std; m)	Snow - Range (std; m)	Canopy - Sill (std; m^2)	Snow - Sill (std; m^2)
K west	4.4 (0.1)	11.6 (0.2)	31.7 (0.4)	0.016 (0.000)
K east	5.5 (0.1)	10.3 (0.1)	35.6 (0.3)	0.033 (0.000)
F west	8.0 (0.1)	7.7 (0.1)	33.3 (0.2)	0.017 (0.000)
F east	5.5 (0.1)	7.5 (0.2)	22.5 (0.4)	0.014 (0.000)
N north	3.0 (0.1)	5.3 (0.1)	5.4 (0.1)	0.031 (0.000)
N south	3.0 (0.0)	6.1 (0.1)	7.0 (0.1)	0.032 (0.000)
A	7.3 (0.3)	7.9 (0.4)	15.5 (0.3)	0.023 (0.001)

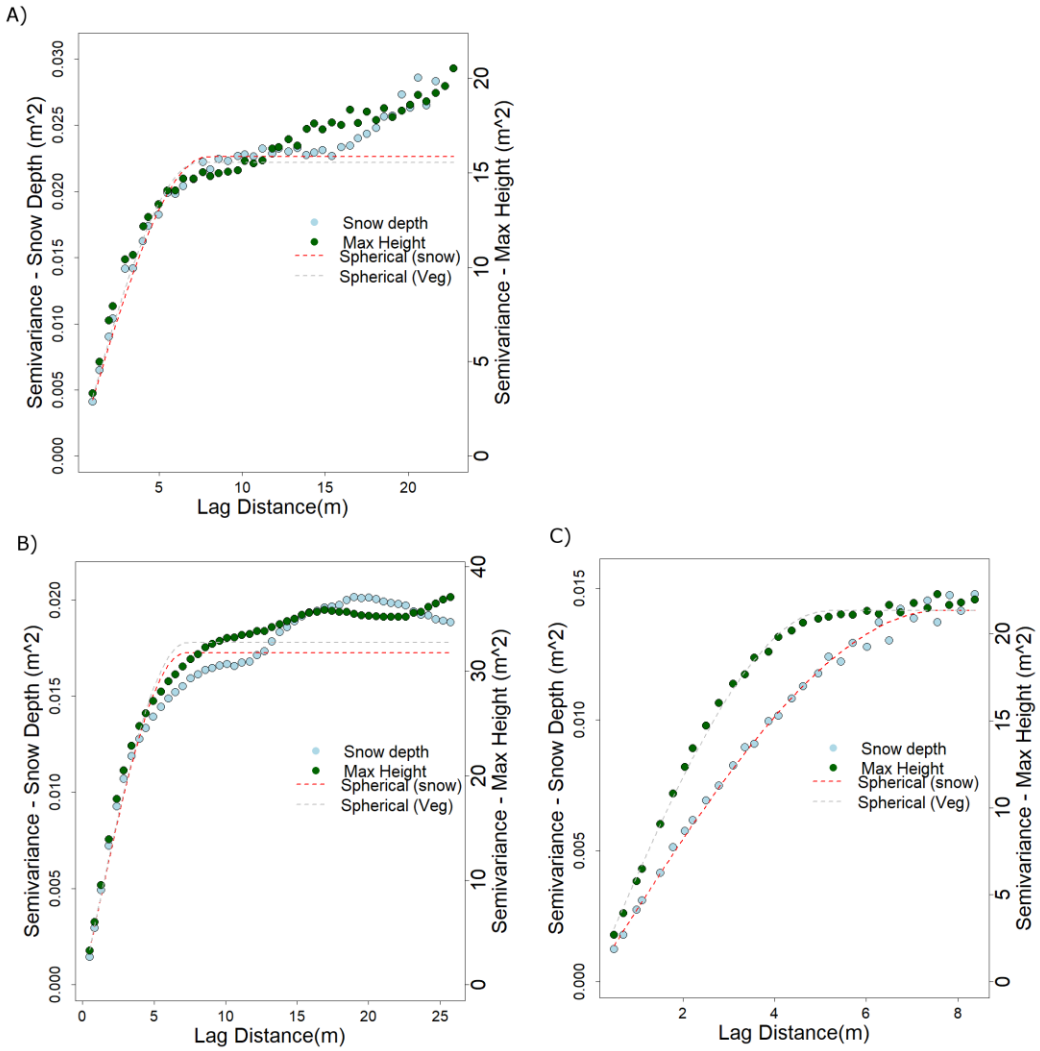

Figure 3.10: Variograms for Sites A and F using snow depth and max height. A) Site A. B) Site F - west. C) Site F - east

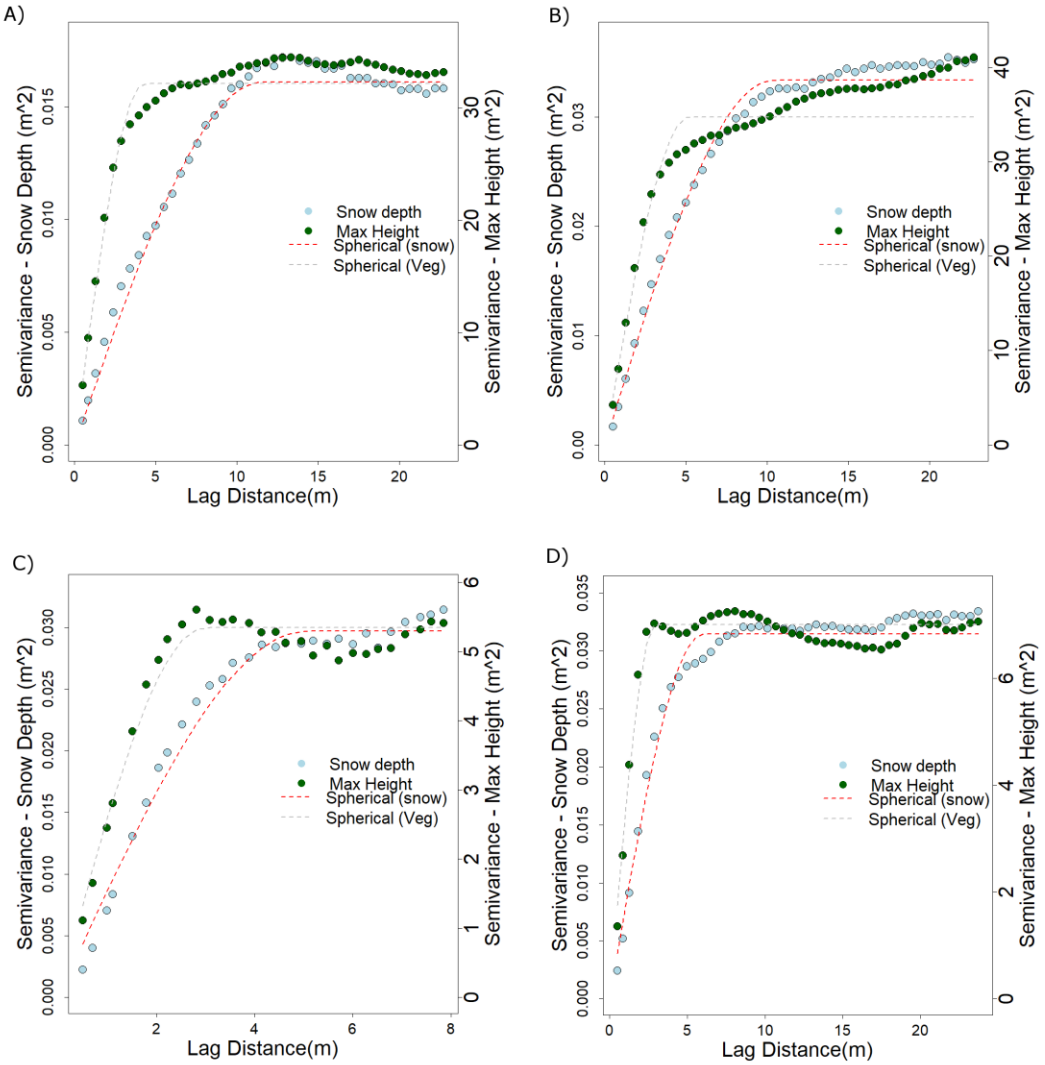

Figure 3.11: Variograms for Sites K and N. A) Site K - west. B) Site K - east. C) Site N - north. D) Site N south.

Canopy vs. Open

Open areas at all sites had deeper snow than in the canopy (Table 3.4). The ratio of canopy:open was identical between Sites K and F (Table 3.5), and nearly identical between Sites A and N.

Table 3.4: Patch list with properties. *Tree heights not found at Site A.

Site	Cover	Description	Area (m^2)	Snow Depth (cm)	Tree Height (m)	Fractional Cover (%)
K	Tree	West	2510	117	21.2	83.9
K	Tree	East	4644	133	16.6	69
K	Grass	Open	3641	185	NA	NA
F	Tree	Big	4380	118	20.7	95.4
F	Tree	Small (East)	691	86	21	100
F	Grass	Open	7329	69	NA	NA
N	Tree	Big (South)	1712	152	10.2	56.5
N	Tree	Small (North)	443	132	10	76.1
N	Grass	Open	913	169	NA	NA
A	Tree	Dense	1335	80	NA*	95.5
A	Shrub	Shrub/Grass	5454	93	NA*	NA

Table 3.5: Ratio of snow depth under canopy to open

Site	Ratio (canopy : open)
K	0.68
F	0.68
A	0.86
N	0.84

Discussion

Overall, pixel-level correlation between snow depth and forest canopy metrics was modest, with maximum canopy height (*max*) having the best correlation to snow depth for almost all sites and pixel sizes. Sub-meter spatial resolution ($0.5m^2$) significantly improved the relationship at Site N (r^2 = 0.42 to 0.51). At the other three sites, 1-3m spatial resolution was optimal. At the patch-level, we found very strong relationships between mean patch lidar metrics and snow depth across Grand Mesa (r^2 = 0.90). 35 statistical descriptors of vertical tree structure were tested, along with stand

characteristic measures. Results support a strong correlation for many metrics. The best vertical distribution metric, FHD, had only slightly stronger correlation with snow depth than fractional cover (R^2 = 0.94 and 0.92 for FHD and fractional cover, respectively; Figure 3.8). The performance of percent fractional cover suggests that tree height, size and individual tree density minimally affect interception at the patch-scale. However, the sample size was small (n=7) and spatial autocorrelation was not addressed. Patches within each site were orders of magnitude closer in distance to each other than patches across sites (tens to hundreds of meters vs. kilometers). Spatial autocorrelation in forest properties (i.e. mean height) and snow depth was observed (similar mean depths and mean canopy metric values at neighboring patches; Figure 3.8), as these properties are driven by spatially correlated site properties like wind and temperature.

As opposed to patch-level, the pixel-level analysis was purely focused on snow distribution directly underneath canopy cover. This approach does not incorporate direct or indirect measures about the patch density, fractional cover or spacing between trees. Visually comparing snow and canopy rasters (Figure 3.5 and 3.6), and their distributions (Figure 3.12) did not reveal any consistent pattern to explain disparities in correlation success between sites. Snow distributions appeared mostly normal at all sites, however sample sizes were too large to test for normality using common normality tests (Shapiro-Wilkes test the Kologorov-Smirnov test). Sites A and F had nearly the same mean snow depth (~80cm), approximately 65% and 55% that of Sites K and N, respectively. To compare snow depth distributions among sites, statistics were normalized to the respective site mean (Table 3.6). The coefficient of variation (CV) of snow depth, a measure of the normalized variation, shows that sites with low pixel-level correlation

(Sites A and F) have more relative variation in snow depth than sites with the highest pixel-level correlation (Sites K and N; Table 3.6). Therefore, there was variation in snow depth which the pixel-level analysis was unable to explain. Other statistical distribution measures are shown for comparison, including interquartile range and skewness.

Table 3.6: Snow depth distribution statistics

Site	Mean (m)	Standard deviation (m): (Coefficient of variation [CV])	IQR (m)	IQR difference (m): (standardized to mean)
K	1.30	0.20 (0.15)	1.17 - 1.44	0.27 (0.21)
F	0.84	0.15 (0.18)	0.74 - 0.94	0.20 (0.25)
A	0.81	0.17 (0.21)	0.71 - 0.89	0.18 (0.23)
N	1.51	0.20 (0.13)	1.36 - 1.67	0.32 (0.21)

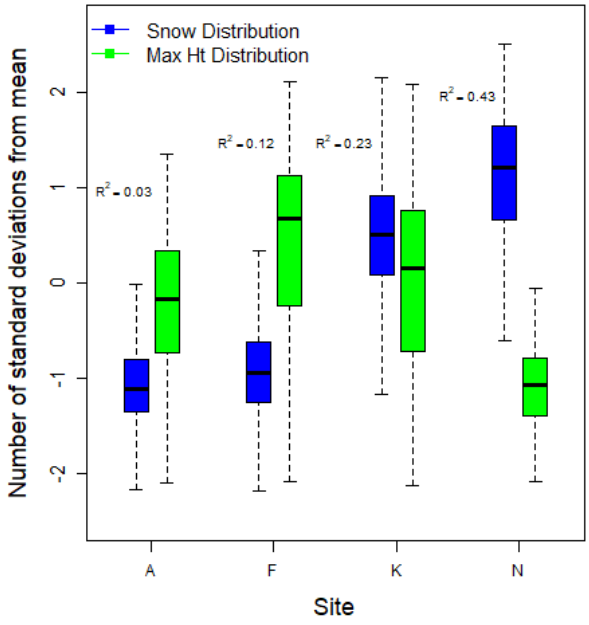

Figure 3.12. Distribution of snow depth and maximum canopy height (max) of 1m2 pixels for patches at each site (pixels combined for sites with two patches). Values standardized by the mean across sites – i.e. snow depth by the mean snow depth of all sites, and max by mean of max. Interquartile range and mean shown in boxes; wings extend to outliers.

Average measured tree height was approximated at each site to determine whether tree height was a first-order cause of pixel-level correlation. As we were unable to identify individual trees at Site A, the average of *max* was used as a surrogate for measured tree height. As opposed to the patch metrics, this average did not incorporate cells without canopy values, therefore this should correlate well to the measured tree sizes. This measure was also uninformative; there was no trend indicating that patch tree height determines pixel-level correlation. However, Site N had the shortest trees and substantially higher pixel-level correlation than the other three sites. Its distinct species composition, spatial distribution and size is in stark contrast to the dense clusters of the taller, older fir and spruce present elsewhere on Grand Mesa. This is perhaps where the pixel-level approach failed to explain the observed variability in snow depth; spatial distribution of trees is not incorporated.

The variogram analysis highlighted the similarity between canopy and snow distribution, both qualitatively and quantitatively. In particular, range parameters of snow depth and vegetation drawn from the experimental variogram models were similar at most sites. Site N had a short range, and distinctly sharp rise to the sill for vegetation which is a reflection of the forest topography and spacing at Site N, and in contrast to Sites A and F particularly. While without the same variogram shape, a more gradual approach to the sill, Site K has the next shortest canopy range values (note: Site F east is tied with Site K east for the fourth shortest range [range = 5.5m]). However, the range in the snow depth variogram is much larger for Sites N and K relative to the canopy variogram. The ratio of snow to canopy ranges for the two patches at Sites K and N are 2.6, 1.9, 1.8 and 2.0, respectively. The ranges for the remaining sites, F west, F east and

A, are 1.0, 1.4 and 1.1, respectively. These results indicate that the canopy and snow spatial distribution have very similar scaling properties (i.e. correlation length), particularly at the denser sites (Sites A and F).

The canopy:open ratio was promising, if not confounding. Sites K and F had identical ratios and similar patch configuration and overall forest stand characteristics. They are from very similar landscapes: patchy forest landscape with expansive open areas and continuous irregularly shaped patches. Site F is further west and is directly exposed to large open areas to the east and north. Site K is a sheltered, u-shaped enclosure which opens to the north, into a large, ~500-1000m wide, open area. Snow depth in the open patch at Sites F and K are 118cm and 185cm respectively. Despite Site F having a much shallower snowpack than Site K (60% less average snowpack), their ratios of canopy:open snow depth is identical. Sites A and N also had nearly identical ratios. Site A contains the westernmost forest patch on Grand Mesa, and has a massive snow drift at a south-facing leeward edge and accompanying shallow scour zone along its windward edge, with a snow depth distribution in the open tracking the overlaying shrub patches in the open. Site N on the other hand has more loosely clustered trees with small treeless openings. The trees are on average much shorter at Site N (approximately 10m). Snow pits within the vicinity of Sites A, F and K showed negligible snow density differences between the canopy and the open, indicating that there is more SWE in the open at Grand Mesa than under the canopy, due to depth differences not density. This agrees with Musselman et al. (2008) who found much smaller snow density differences relative to depth difference based on distance from tree bole. However, an analysis of all pits across Grand Mesa was not undertaken for this study. More TLS sites would be

necessary, along with observations closer to the date of maximum SWE to generalize this finding to Grand Mesa or similar cold regions.

As snow depth scans were taken in February, when no significant melt was observed in snow pit observations at Grand Mesa, interception should be responsible for intracanopy and canopy to open snow depth variation. Per modelled results from Hedstrom et al. (1998), higher wind speeds can functionally turn a canopy that is not fully-closed into a closed canopy – i.e. the effective canopy cover becomes "unity." Horizontal wind speed can transport falling snow from openings into the lower branches after they enter canopy interspace. Sites F and A had near maximum fractional cover to begin with. It is possible that tightly-packed forests with near unity canopy cover have a more uniform range of canopy interception efficiency (CIE) across the patch. This is a plausible explanation for the lack of pixel-level correlation between snow depth and canopy metrics at Sites F and A, the two most exposed and windy sites. Three of our sites were distinctive subalpine climax communities with rigid-needled, patchy forest structures typical of the region, while Site N was well-spaced, short-statured second growth pine. In addition to the spatial distribution differences, pine has much lower tree-level CIE as compared to subalpine species (Hedstrom et al., 1998). Pixel-level correlation was relatively strong at this site suggesting good application at disturbed, second-growth locations. Given the inconsistent pixel-level results across patches and the strong similarities between canopy and snow depth spatial distribution from variogram analysis, the greatest utility of forest canopy data in snow accumulation modelling might be a subgrid parameterization of SWE based on stand-level geostatistical properties of the forest, e.g. snow depletion curves (Luce et al., 1999).

Taking into account the limited sample size of patches, fractional cover may not sufficiently explain snow depth variation in many circumstances and additional height and vertical distribution metrics may be necessary. That simple binary canopy cover had an r^2 above 0.90 at the patch-level indicates that other sources of remotely-sensed data capable of measuring two-dimensional fractional cover may be adequate for modelling interception in large-scale snow models. However, binary measures derived from optical imagery are only superficial characteristics of the upper layer of the canopy. Radiative energy fluxes may be significantly more sensitive to spatial gradients in structural forest canopy attributes than the interception processes observed during this study.

Conclusions

This study used TLS point clouds collected at four sites across Grand Mesa, CO, to investigate the effect of forest canopy properties on snow depth during the snow accumulation period in February, 2017. Correlation analysis was performed at multiple scales to determine the optimal scale to represent snow and forest canopy interactions. Strong correlation was found between canopy cover and snow depth at the forest patch-scale for a small number of samples (n=7 patches). Weighting canopy cover with vertical distribution metrics of the canopy (i.e. maximum height, standard deviation, etc.) only minimally improved the patch-level correlation (from $r^2 = 0.92$ to $r^2 = 0.94$). Pixel-level correlation was relatively lower with $r^2 = 0.03$ to $r^2 = 0.51$, but at a much more robust sample size. Denser sites, or those with more canopy cover had very low correlation at the pixel scale. The second growth pine site showed the best correlation ($r^2 = 0.51$), indicating that vertical distribution metrics derived from point clouds have utility in gridded, spatially distributed snow models as snow depth correction factors under sparse

forests. The $0.5m^2$ pixel size at Site N significantly improved the correlation compared to the $1m^2$ size ($r^2 = 0.40m^2$), but decreased at finer resolutions indicating that approximately meter scale resolution is optimal for subcanopy snow modelling whereas relationships fall apart at the centimeter scale. The similarity in scaling properties between collocated canopy and snow distributions drawn from variogram analysis, and the consistent canopy:open ratio, could prove useful information in models using subgrid parameterization where forest cover data is present.

References

Blöschl, G. (2001). Scaling in hydrology. *Hydrological Processes*, *15*(4), 709-711.

Broxton, P. D., Harpold, A. A., Biederman, J. A., Troch, P. A., Molotch, N. P., & Brooks, P. D. (2015). Quantifying the effects of vegetation structure on snow accumulation and ablation in mixed-conifer forests. *Ecohydrology*, *8*(6), 1073-1094.

Deems, J. S., Painter, T. H., & Finnegan, D. C. (2013). Lidar measurement of snow depth: a review. *Journal of Glaciology*, *59*(215), 467-479.

Dhakal, S. (2016). *Assessing the limitation and capabilities of lidar and Landsat 8 to estimate aboveground vegetation biomass and cover in a rangeland ecosystem using a machine learning algorithm*. (Unpublished master's thesis). Retrieved from https://drive.google.com/file/d/0B6NXB8xUiBs6dUdUbTBQNXBTLXc/view

Dickerson-Lange, S. E., Lutz, J. A., Gersonde, R., Martin, K. A., Forsyth, J. E., & Lundquist, J. D. (2015). Observations of distributed snow depth and snow duration within diverse forest structures in a maritime mountain watershed. *Water Resources Research*, *51*(11), 9353-9366.

Eysn, L., Hollaus, M., Lindberg, E., Berger, F., Monnet, J. M., Dalponte, M., ... & Pfeifer, N. (2015). A benchmark of lidar-based single tree detection methods using heterogeneous forest data from the alpine space. *Forests*, *6*(5), 1721-1747.

Hall, D. K., Riggs, G. A., & Salomonson, V. V. (1995). Development of methods for mapping global snow cover using moderate resolution imaging spectroradiometer data. *Remote sensing of Environment*, 54(2), 127-140.

Hedrick A.R., Marks, D., Havens, S., Robertson, M., Johnson, M., Sandusky, M., …& Painter, T.H. (2018). Direction insertion of NASA Airborne Snow Observatory-derived snow depth time-series into *iSnobal* energy balance snow model. *Water Resources Research.*

Hedstrom, N. R., & Pomeroy, J. W. (1998). Measurements and modelling of snow interception in the boreal forest. *Hydrological Processes*, *12*(10-11), 1611-1625.

Luce, C. H., Tarboton, D. G., & Cooley, K. R. (1999). Sub-grid parameterization of snow distribution for an energy and mass balance snow cover model. *Hydrological Processes*, *13*(12-13), 1921-1933.

MacArthur, R. H., & MacArthur, J. W. (1961). On bird species diversity. *Ecology*, *42*(3), 594-598.Malanson, G. P., Butler, D. R., Fagre, D. B., Walsh, S. J., Tomback, D. F., Daniels, L. D., ... & Bunn, A. G. (2007). Alpine treeline of western North America: linking organism-to-landscape dynamics. *Physical Geography*, *28*(5), 378-396

Malanson, G. P., Butler, D. R., Fagre, D. B., Walsh, S. J., Tomback, D. F., Daniels, L. D., ... & Bunn, A. G. (2007). Alpine treeline of western North America: linking organism-to-landscape dynamics. *Physical Geography*, *28*(5), 378-396.

Matzarakis, A., & Matuschek, O. (2011). Sky View Factor as a parameter in applied climatology–Rapid estimation by the SkyHelios Model. *Meteorologische Zeitschrift*, *20*(1), 39-45.

McGarigal, K., Cushman, S. A., Neel, M. C., & Ene, E. (2002). FRAGSTATS: spatial pattern analysis program for categorical maps.

Musselman, K. N., Molotch, N. P., & Brooks, P. D. (2008). Effects of vegetation on snow accumulation and ablation in a mid-latitude sub-alpine forest. *Hydrological Processes: An International Journal*, *22*(15), 2767-2776.

Painter, T. H., Berisford, D. F., Boardman, J. W., Bormann, K. J., Deems, J. S., Gehrke, F., Hedrick, A., … & Winstral, A. (2016). The Airborne Snow Observatory: Fusion of scanning lidar, imaging spectrometer, and physically-based modeling for mapping snow water equivalent and snow albedo. *Remote Sensing of Environment*, *184*, 139-152.

Pebesma, E.J., 2004. Multivariable geostatistics in S: the gstat package. *Computers & Geosciences*, 30, 683-691.

Persson, A., Holmgren, J., & Soderman, U. (2002). Detecting and measuring individual trees using an airborne laser scanner. *Photogrammetric Engineering and Remote Sensing*, *68*(9), 925-932.

Pomeroy, J.W., Marks, D., Link, T., Ellis, C., Hardy, J., Rowlands, A. & R. Granger. (2009). The impace of coniferous forest temperature on incoming lnogwave radiation to melting snow. *Hydrological Processes*, *23, 2513-2525*

R Core Team (2017). R: A language and environment for statistical computing. R Foundation for Statistical Computing, Vienna, Austria. URL http://www.R-project.org/

Rango, A. (1993). II. Snow hydrology processes and remote sensing. *Hydrological Processes*, *7*(2), 121-138.

Seyednasrollah, B., & Kumar, M. (2014). Net radiation in a snow-covered discontinuous forest gap for a range of gap sizes and topographic configurations. *Journal of Geophysical Research: Atmospheres*, *119*(17).

Smith, W. K., Germino, M. J., Hancock, T. E., & Johnson, D. M. (2003). Another perspective on altitudinal limits of alpine timberlines. *Tree physiology*, *23*(16), 1101-1112.Vuyovich, C. M., Jacobs, J. M., & Daly, S. F. (2014). Comparison of passive microwave and modeled estimates of total watershed SWE in the continental United States. *Water Resources Research*, *50*(11), 9088-9102.

Solberg, S., Naesset, E., & Bollandsas, O. M. (2006). Single tree segmentation using airborne laser scanner data in a structurally heterogeneous spruce forest. *Photogrammetric Engineering & Remote Sensing*, *72*(12), 1369-1378.

Vauhkonen, J., Ene, L., Gupta, S., Heinzel, J., Holmgren, J., Pitkänen, J., ... & Lien, V. (2011). Comparative testing of single-tree detection algorithms under different types of forest. *Forestry*, *85*(1), 27-40.

CONCLUSION

The purpose of this thesis was to investigate the effect of forest canopy on snow depth distribution, both in the subcanopy and in open areas abutting the forest. The majority of spatial distribution patterns of SWE are controlled by vegetation and topography. While abnormal synoptic weather occurs, fractional snow melt patterns are generally consistent interannually, and share scaling properties with these landscape features. The translation of fundamental, process-based forest snow relationships into general forest structure properties that can be measured via remote-sensing is crucial.

The first study characterized snow depth near the canopy based on distance to forest edge, and the direction the edge was oriented. Using these and common topographic metrics, multilinear models were tested for effectiveness in characterizing wind redistribution of snow near the forest. Model results were interpreted with the assumption that in mid-winter, snow distribution patterns would be due to wind redistributive processes. This methodology was applied at three sites across the mesa. Preferential snow distribution along the prevailing wind path was indicated by both explicit and implicit edge direction representations at one site. Log-transformed *distance from edge* performed well at a sheltered site, indicating a uniform edge effect due to interception.

The second study uses four sites to characterize the subcanopy snow distribution and relate it to the vertical distribution of forest in the overstory and various other forest properties. Two of the sites are the same as the first study. Analysis was performed on the

pixel scale, and a larger forest patch scale. Canopy metrics were only predictive at sites with less fractional forest cover – i.e. discontinuous and second-growth forests. Minimal correlation was observed at the two sites with near continuous canopy cover. Variation in snow depth was equivalent between all sites, indicating that the pixel-level approach did not explain the variation in snow depth in dense forest. Geostatistical analysis showed that the spatial distribution of snow was closely aligned with that of the forest canopy, even in sites with poor pixel-level correlation. Patch-level correlation was very strong, albeit using an analysis with small sample sizes (n=7), but the benefit of adding vertical canopy distribution information was minimal. Additionally, the ratio of snow depth in the canopy to snow in the open remained consistent between two of the sites with the most similar canopy characteristics. Snow was shallower under the canopy compared to the open at all sites. These outcomes suggest that data on forest cover is important for adjusting subcanopy SWE, and that the requirement for vertical forest structure information in modelling snow accumulation depends on the model type and spatial resolution, and forest properties of the model domain.

This experiment was designed in large part as ground validation for aerial remote sensing products such as airborne lidar. Due to logistics and cost, only one repeat measurement at most was made at each site, during which time period, only a small amount of snow had fallen. Similar snow studies in the future would benefit from collecting data over an entire snow season, or specifically during either the accumulation or ablation period. Additional TLS-derived measures such as biomass or leaf area index may also be insightful for dense canopy sites where we observed very weak pixel-level correlation to canopy metrics.

APPENDIX A

Model Coefficients and Effect Size Tables

Table A.1: Site K Model 11.

Variable (Categorical)	Intercept (cm)	Coefficient of Variation	P-value
N	144	0.01	0.00
NE	136	0.28	0.00
E	138	0.35	0.01
SE	146	1.00	0.39
S	151	0.33	0.09
SW	151	0.35	0.09
W	138	0.35	0.01
NW	143	2.09	0.29
Variable (Continuous)	**Coefficient**		
N: distance	0.09	0.09	0.00
NE: distance	0.08	0.85	0.36
E: distance	0.09	6.41	0.31
SE: distance	0.03	0.17	0.00
S: distance	0.02	0.13	0.00
SW: distance	0.05	0.25	0.01
W: distance	0.10	0.85	0.15
NW: distance	0.10	0.97	0.22

Table A.2: Site F Model 7.

Variable (Categorical)	Intercept (cm)	Coefficient of Variation	P-Value
N	129	0.01	0.00
NE	110	0.11	0.00
E	105	0.05	0.00
SE	115	0.08	0.00
S	119	0.14	0.00
SW	118	0.09	0.00
W	103	0.07	0.00
NW	122	0.13	0.00
Variable (Continuous)	**Coefficient**		
Concavity *	6.9	0.12	0.00
N: distance	-0.0017	0.02	0.00
NE: distance	0.0040	0.16	0.00
E: distance	0.0065	0.08	0.00
SE : distance	0.0040	0.10	0.00
S: distance	0.0006	0.41	0.11
SW :distance	0.0009	0.15	0.00
W : distance	0.0086	0.10	0.00
NW: distance	-0.0026	0.30	0.03

Table A.3: Site O Model 18

Variable	Coefficient	Coefficient of Variation	P-Value
[Intercept]	1.62	0	0.00
Slope	0.007	0.14	0.00
Aspect	-0.014	0.55	0.12
Slope * Asp	0.026	0.05	0.00

Vegetation and Patch Metric Lists

Table A.4: Vegetation Metrics (BCAL).

Metric Abbreviation	Metric Name
min	Minimum Height
max	Maximum Height
range	Height Range
mean	Mean Height
mad	Median Absolute Deviation (MAD) from Median Height
aad	Mean Absolute Deviation from Mean Height
var	Height Variance
std	Standard Deviation
skw	Skewness
kurt	Kurtosis
intrqrtle	Interquartile Range (IQR) of Height
coefvar	Height Coefficient of Variation
per_5th	Height Percentiles (5^{th})
per_10th	Height Percentiles (10^{th})
per_25th	Height Percentiles (25^{th})
per_50th	Height Percentiles (50^{th})
per_75th	Height Percentiles (75^{th})
per_90th	Height Percentiles (90^{th})
per_95th	Height Percentiles (95^{th})
lid_ret	Total lidar points within each pixel
lid_veg_ret	The total number of all the points within each pixel that are above the specified crown threshold value (CT).
lid_grd_ret	The total number of all the points within each pixel that are below the specified ground threshold value (GT).
veg_ven	The percent ratio of vegetation returns and ground returns within each pixel. Density = nV/nG*100
veg_cov	The percent ratio of vegetation returns (nV) and total returns within each pixel.
grd_rtn_pct	The percent ratio of ground returns (nV) and total returns within each pixel.
pct_veg_0	Percent of vegetation in height ranges 0-1m within each pixel
pct_veg_1	Percent of vegetation in height ranges 1-2.5m within each pixel
pct_veg_2	Percent of vegetation in height ranges 2.5-10m within each pixel
pct_veg_10	Percent of vegetation in height ranges 10-20m within each pixel
pct_veg_20	Percent of vegetation in height ranges 20-30m within each pixel
pct_veg_30	Percent of vegetation in height ranges >30m within each pixel
CRR	Canopy relief ratio of points within each pixel. Canopy relief ratio = ((HMEAN - HMIN))/((HMAX - HMIN))
text	Texture of height of points within each pixel. Texture = St. Dev. (Height > Ground Threshold and Height < Crown Threshold)
FHD_All	Foliar height diversity (FHD) of all points
FHD_ab_grd	Foliar height diversity (FHD) of above ground points

Table A.5: Patch metrics.

Metric Abbreviation	Metric Name and Description
area	Patch area
perimeter	Length of patch perimeter
tree_count	Total number of trees contained in patch
height_avg	Mean height of all trees in patch
height_std	Tree height SD of all trees in patch
tree_density	Trees/hectare in patch

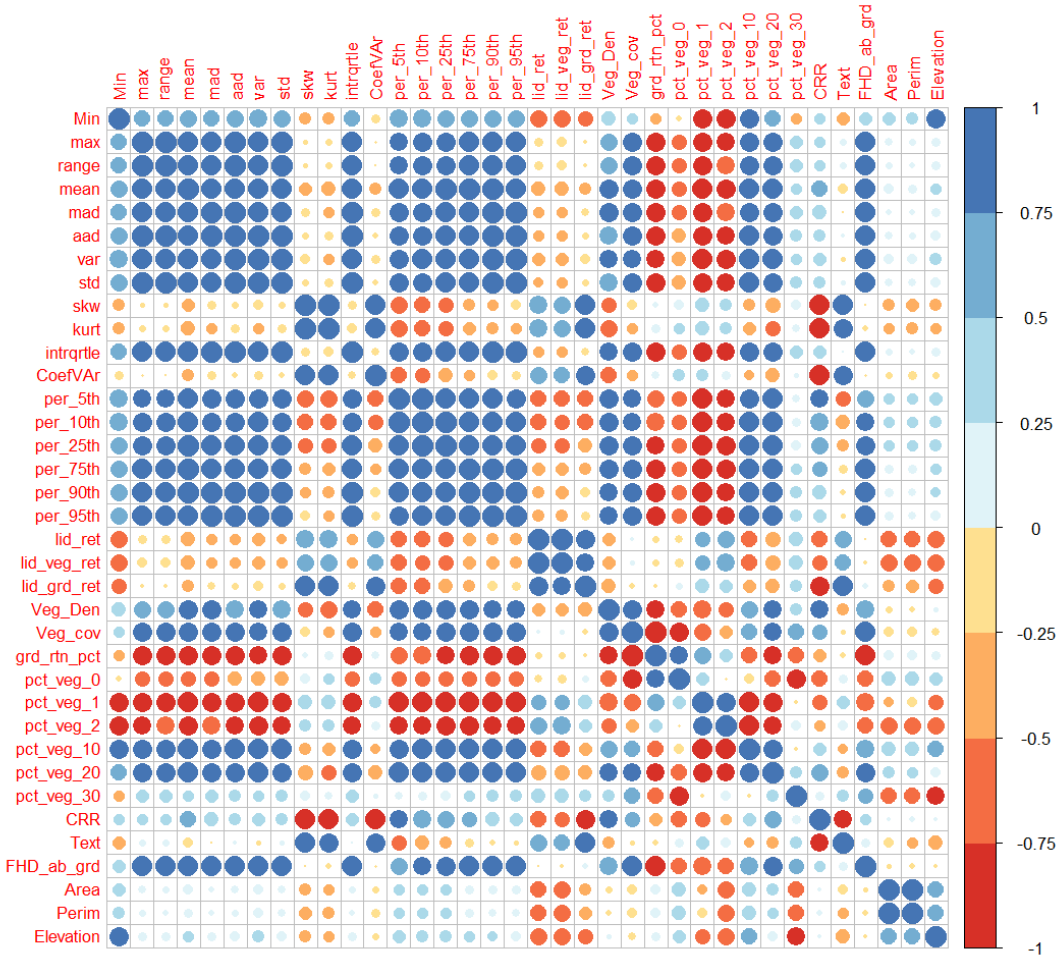

Figure A.1: Covariance matrix from patch analysis.